RSC Advances

This is an *Accepted Manuscript*, which has been through the Royal Society of Chemistry peer review process and has been accepted for publication.

Accepted Manuscripts are published online shortly after acceptance, before technical editing, formatting and proof reading. Using this free service, authors can make their results available to the community, in citable form, before we publish the edited article. This *Accepted Manuscript* will be replaced by the edited, formatted and paginated article as soon as this is available.

You can find more information about *Accepted Manuscripts* in the Information for Authors.

Please note that technical editing may introduce minor changes to the text and/or graphics, which may alter content. The journal's standard Terms & Conditions and the Ethical guidelines still apply. In no event shall the Royal Society of Chemistry be held responsible for any errors or omissions in this *Accepted Manuscript* or any consequences arising from the use of any information it contains.

ROYAL SOCIETY OF CHEMISTRY

www.rsc.org/advances

Journal Name

RSCPublishing

ARTICLE

Three dimensional metal oxides–graphene composites and their applications in lithium ion batteries

Cite this: DOI: 10.1039/x0xx00000x

Received 00th January 2012,
Accepted 00th January 2012

DOI: 10.1039/x0xx00000x

www.rsc.org/

Jiantao Zai and Xuefeng Qian*

Due to the huge energy and environment problems caused by the use of fossil fuels, R&D on innovative energy storage systems never become so important as today. Although there still are some safety, energy, power and cost issues, electric vehicles become more and more commonly in our daily life, such as E–bike or E–car. This paper provides an overview of recent progress on three dimensional (3D) metal oxides–graphene (MOs–G) composites as advanced electrode materials in lithium ion batteries (LIBs). Beginning with the brief description of the importance and preparation methods of 3D MOs–G composites, the effects of the morphology and size of metal oxides (MOs) or graphene on composites for LIBs are then systematically reviewed and discussed. Additionally, the important effects of composition and interactions between metal oxides and graphene are also pointed out. Finally, future challenges of MOs–G composites for lithium ion batteries are discussed.

1 Introduction

Reports from Chinese Academy of Social Sciences indicate that more than 130 million vehicles are in China in 2013, and the number is expected to be 400 million (one car per family) in the future[1]. These vehicles have created massive traffic jams and considered as one of the main reasons of poor air quality in China. It is hard to image our future life if all the increasing 270 million vehicles are based on fossil fuels. These problems are not just for China but also for all the world. It is no doubt that the development of electric vehicles (EVs) must be one of the good choices. EVs have become more and more commonly in our daily life, for instance, e–bikes are widely used in both city and countryside in china. But the popularization of EVs is always limited by the safety, cost, cruising ability and power. To overcome these issues, people have started to expect better electrochemical performances from lithium ion batteries (LIBs).[2-8] However, the development of better safety, higher energies and power densities in LIBs is meeting some technical bottlenecks at present stage.

Graphene is a two–dimensional (2D) sheet of sp^2 bonded carbon atoms in a hexagonal honeycomb lattice, which can be viewed as an extra–large polycyclic aromatic molecule.

Dr. Jiantao Zai *received Bachelor (2007) and Ph.D. (2012) degree in applied chemistry from Shanghai Jiao Tong University, then worked with Prof. Donghai Wang in Penn State University. He joined SJTU as Lecturer in 2014. His research interests include the synthesis chemistry of Group IV inorganic materials and their potential applications in energy storage, photovoltaic and photocatalytic areas. He is honored to receive the 2014 Shanghai Chenguang project, 2012 Shanghai outstanding graduates and 2012 Scholarship of Sinopoly Battery Ltd.*

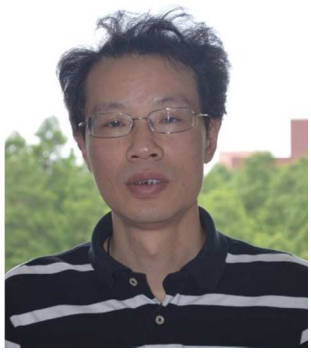

Prof. Xuefeng Qian *worked in School of Chemistry and Chemical Engineering, Shanghai Jiao Tong University. He received Bachelor degree from HeFei University of Technology (1990), Master (1995) and Ph.D (1998) degrees from USTC. He is interesting in the design, synthesis, and applications of materials related with solar utilizations and energy storage. He was awarded 2008 Outstanding University Young Teachers in Shanghai, 2006 New Century Excellent Talents of Education Ministry of China.*

RSC Advances Accepted Manuscript

Graphene nanosheets (GNSs) have been known to be components of traditional carbon materials (e.g. graphite) or components of a ''new'' class of carbon materials (such as carbon nanotubes). The discovery of monolayer graphene can be tracked to the 1960s and 1970s.[9] Then graphene with the size only in tens nm on an appropriate substrate (crystal surfaces of transition metals and metal carbides) was successfully fabricated by Oshima and Nagashima in 1997 through decomposing hydrocarbon gases at high temperature.[10] Ruoff, R. S. also did pioneer works on tailoring graphite with the goal of achieving single sheets.[11] After being firstly transferred to a SiO_2 substrate by Geim and Novoselov in 2004, the field effect of graphene was demonstrated.[10-12] The ideal GNSs achieved by a mechanical exfoliation technique have proven to be highly ordered, outstanding surface areas (2630 $m^2 g^{-1}$), high Young's modulus (1 TPa), high thermal conductivity (5000 W mK^{-1}), strong chemical durability and high electron mobility (2.5×10^5 $cm^2 V^{-1} s^{-1}$).[13-15]

Since chemical exfoliation method was developed to produce graphene at low cost and in a large quantity,[16] graphene has been widely applied in polymer composites,[17] transistors,[18, 19] optoelectronics,[20, 21] memory device,[22, 23] sensors (gas-,[24, 25] bio-,[26] electrochemical-[27] and chemical-[28]), solar cells,[20, 29] field emission devices,[30, 31] catalysts,[31] photocatalysts,[14, 32] nanogenerators,[33] hydrogen storage,[34] CO_2 capture,[35] and etc. Especially, graphene–based electrochemical storage devices (e.g. high–performance LIBs) have attracted much attention in fundamental studies and practical applications with greatly improved electrochemical performances due to its unique 2D structure and excellent physiochemical properties.[3, 4, 36-44] Furthermore, the graphene–based electrochemical storage energy devices do not need high quality graphene without any defects like electronics, and graphene produced by chemical exfoliation method, such as reduced graphite oxide (RGO) with many defects and multiple layers, can also meet the demands of high–performance LIBs.

Detailed descriptions of the properties, synthesis, functionalization and applications in energy storage areas of graphene and its composites can be found in recent papers.[3-5, 17, 29, 36, 38-52] For example, Wu et al. have reviewed systematically the pros and cons of graphene and metal oxides, and focused on the synergistic effects of metal oxides-graphene composites on improving the electrochemical properties of LIBs and electrochemical capacitors.[49] Here, we provide an overview of the recent progress in three–dimensional (3D) metal oxides–graphene (MOs–G) composites as advanced lithium storage materials for high–performance LIBs since 2012, especially focus on the important effects of morphologies, composition, interactions between metal oxides (MOs) and graphene on the improvement of their electrochemical properties, including capacity, rate capability and cyclic stability.

2 3D metal oxides–graphene composites

2.1 Why using 3D MOs–G composites

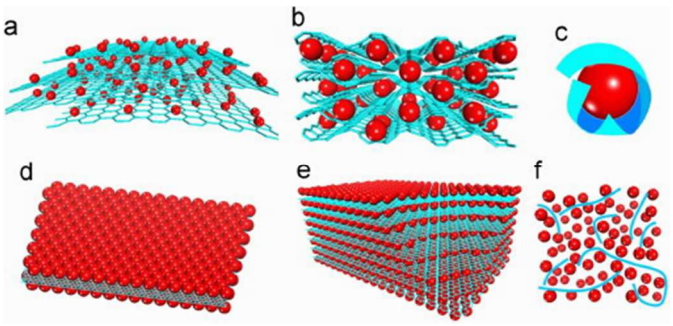

Figure 1. Schematic of structural models of MOs–G composites: (a) Anchored model: nanosized MOs particles are anchored on the surface of graphene. (b) Wrapped model: MOs particles are wrapped by graphene. (c) Encapsulated model: MOs particles are encapsulated by graphene. (d) Sandwich–like model: graphene serves as a template for the creation of a MOs/graphene/MOs sandwich–like structure. (e) Layered model: a structure composed of alternating layers of MOs nanoparticles and graphene. (f) Mixed model: graphene and MOs particles are mechanically mixed and graphene forms a conductive network among MOs particles. Red: MOs particles; Blue: graphene sheets.[49] Reproduced from Ref. [49], Copyright (2012) with permission from Elsevier.

Due to its special 2D structure, graphene has a high Li^+ ions storage capacities, 1116 mAh g^{-1} based on LiC_2 model[53] or 744 mAh g^{-1} based on Li_2C_6 model[54]. But the graphene based electrodes usually show poor stability for the restacking of graphenes.[37] While MOs with high theoretical reversible capacities (such as 717 mA h g^{-1} of NiO, 1007 mA h g^{-1} of Fe_2O_3, 755 mA h g^{-1} of MnO, 890 mA h g^{-1} of Co_3O_4) will suffer from huge volume changes during continuous charge/discharge processes, which would lead to the rapid disintegration of anodes and capacity fading upon cycling. Furthermore, the lower electronic conductivity of MOs is another disadvantage. These problems can be greatly overcomed by combining MOs with graphene to form composites with multiple synergistic effects. Wu et al.[49] summarized these synergistic effects as following: (i) graphene is a novel 2D support for the uniform nucleating, growth or assembling of MOs with well–defined size, shape and crystallinity; (ii) MOs between the layers of graphene can efficiently suppress the re–stacking of graphene; (iii) graphene can act as a 2D conductive template for building a 3D interconnected conductive porous network to improve the electrical conductivity and charge transport of pure oxides; (4) graphene can suppress the volume change and particle agglomeration of MOs during the charge–discharge process; (5) oxygen–containing functional groups on graphene ensure good interfacial interactions and electrical contacts between graphene and MOs.

3D hierarchical structures in micro or sub–micro size, assembled by simple low dimensional nano–sized building blocks, can avoid the aggregation of anode materials and are benefit to the electrode fabrication process.[55-58] The 3D hierarchical structures can also supply more sites to connect with conductive matrix (such as graphene, conductors or current collectors) and keep the activity of Li storage materials during cycling. Besides, 3D hierarchical structures have additional benefits to greatly improve the electrochemical

RSC Advances Accepted Manuscript

This journal is © The Royal Society of Chemistry

performance of electrode materials in LIBs, they also have other special effects[56-58]: the opening porous structures in 3D–hierarchical structures are readily accessible for electrolyte, facilitating the transportation of Li^+ ions from liquid to active surface of active materials. Second, nanosized building blocks of 3D hierarchical structures can significantly shorten the diffusion distance of Li^+ ions and therefore significantly enhance the lithium insertion–extraction kinetics. Third, the 3D hierarchical structures with plenty of pores can accelerate phase transitions and restrain the crumbling and cracking of electrodes, leading to superior cycling performance. In addition, the well–connected 3D hierarchical structures with large surface area can reduce the concentration polarization and facilitate the electron transportation, which accounts for the high rate performance.

Up to now, several structural models of MOs–G composites have been developed, such as anchored, wrapped, encapsulated, sandwich–like, layered and mixed models (**Figure 1**)[49]. Due to the large surface area and restacking nature of graphene, most graphene composites are in 3D hierarchical structures. These 3D MOs–G composites can combine the synergistic effects of graphene composites and benefits derived from 3D hierarchical structures together. Thus they would possess better long–term stability and rate capability than pure 3D hierarchical MOs and graphene composites with simple structure, such as anchored model or sandwich–like model.

2.2 How to get 3D MOs–G composites

The fabrication of graphene or graphene oxide is the first stage to prepare 3D MOs–G composites. Up to now, graphene can be fabricated by various methods, such as chemical vapor deposition (CVD), plasma–enhanced CVD, epitaxial growth on electrically insulating surfaces, electric arc discharge and solution–based chemical oxidation–reduction process.[3, 59-61] For the aim of industrialization and preparing graphene composites, the fabrication method should be easily scalable for the large–scale production of graphene firstly. And then the obtained graphene or its precursors must be easily processable with other active materials. Thus, the most promising method is the chemical oxidation of graphite, conversion of the resulting graphite oxide to graphene oxide (GO), and the subsequent reduction of GO.[16, 62] The method can produce GO and RGO in large scale and realize the industrialization process. Furthermore, abundant oxygen–containing functional groups, such as carboxyl, hydroxyl, epoxy and keto groups, make GO dispersible in water and organic solvents, interactive with metal ions and various compounds by electrostatic interaction and/or chemical bonds.[4, 5, 14, 46, 49, 51, 63, 64] Furthermore, the structure, electrical conductivity and electrochemical performance of RGO are mainly determined by the reduction methods of GO, including chemical, thermal, electrochemical and photo–irradiation techniques, which have been reviewed well by Kuila et al.[40]

Once the large–scale production of graphene by chemical oxidation of graphite is realized, physical mixed method is considered to be one of the most simple and convenient methods to fabricate 3D MOs–G composites. In this method, graphene, usually in RGO, is previous prepared according to above methods and dispersed into water or other solvents to form a

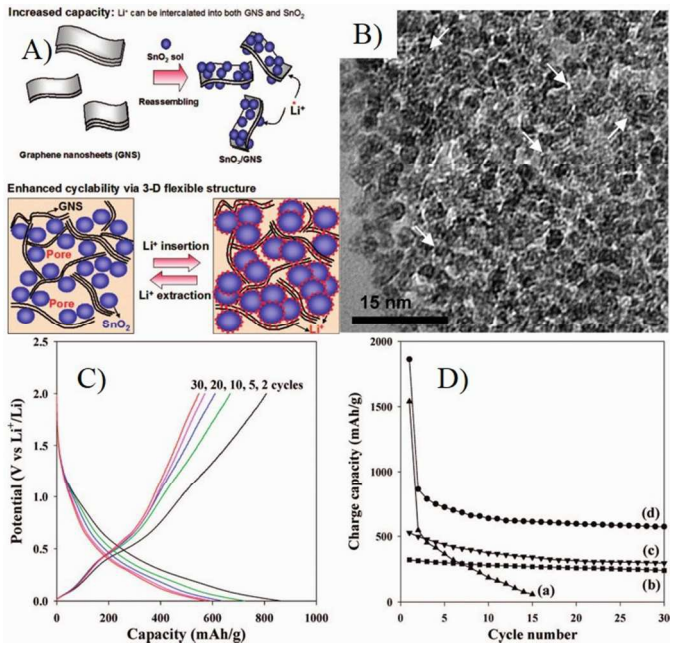

Figure 2. A), Schematic illustration for the synthesis and the structure of SnO_2/GNS; B), TEM image of SnO_2/GNS, the white arrows denote the GNSs; C), charge/discharge profile for SnO_2/GNS; D), cyclic performances for (a) bare SnO_2 nanoparticle, (b) graphite, (c) GNS, and (d) SnO_2/GNS.[65] Reproduced with permission from Ref. 65 Copyright (2009) American Chemical Society.

suspension, then mixed with the pre-fabricated MOs by ultrasonic treatment or stirring process, and MOs–G composites are obtained followed by flocculation, filtration, centrifugation or freeze–drying process. In the pioneer work of Paek et al.[65] (**Figure 2**), RGO was prepared via the chemical reduction of exfoliated graphite oxide, and SnO_2 nanoparticles were obtained by the controlled hydrolysis of $SnCl_4$ with NaOH, then SnO_2/GNS nanocomposites were obtained by reassembling RGO in the presence of SnO_2 nanoparticles.[65] Since the great developments of MOs nanomaterials with rich compositions and morphologies (0D, 1D, 2D and 3D nanostructures) in past decades, the method has been widely used to fabricate 3D MOs–G composites. For instance, 3D–hierarchical NiO–GNSs composites were prepared by simply mixing 3D–hierarchical NiO carnations with RGO under ultrasonic treatment.[66] Recently, graphene nanocomposites based on bi-metal oxides (e.g. $MnFe_2O_4$[67], $NiFe_2O_4$[68], $CoFe_2O_4$[69]) were also obtained by similar methods. On the other hand, milling method is also a facile industrialized physical mixed method to prepare MOs–G composites.[70, 71]

Due to the abundant oxygen–containing functional groups, GO and RGO are usually negatively charged, and they can easily form composites with positively charged MOs by co–assembly process via electrostatic interactions. But the pre–fabricated MOs are always negatively charged or neutral (e.g. Co_3O_4 and Fe_3O_4 nanoparticles are always terminated by OH

RSC Advances Accepted Manuscript

functional groups[74, 75]), thus MOs are usually modified by grafting method. For example, Feng et al. grafted aminopropyltrimethoxysilane (APS) to OH terminated Co_3O_4 or Fe_3O_4 nanoparticles to render the positively charged oxides in an acidic solution.[74] Beyond APS, various positively charged compounds, such as Poly dimethyl diallyl ammonium chloride (PDDA), (3–aminopropyl) trimethoxysilane (APTMS) and poly(allylamine hydrochloride) (PAH), were also used.[76-79] However, the method is not suitable to metal hydroxides due to their dissolution in acid solution. Zhang et al. described a general strategy to fabricate graphene coated large–area $Co(OH)_2$ heterostructures by assembling the positively charged hydroxide nanosheets and negatively charged functionalized graphene in nearly neutral solution (**Figure 3**A–B).[72] Then they developed a modified method to prepare binder free and mechanically robust CoO/graphene electrodes (**Figure 3**C–D). The negatively charged RGO or GO can also be positively charged by surface grafting, such as amine–functionalized graphene.[80] 3D MOs–G composites fabricated via electrostatic interactions are always in encapsulated and layered models. The large surface area of graphene and strong intermolecular forces between MOs and graphene can make MOs nanoparticles dispersing well on graphene and prevent their aggregation, which are also benefits to the stability and high electrical conductivity of composites. Furthermore, graphene is usually in microscale, which can ensure the self–assembled MOs nanostructures effectively covered or supported by graphene. And the porous nature, generated by co–assembly process, can facilitate the ion diffusion and accommodate the volume change during the cycle processes.

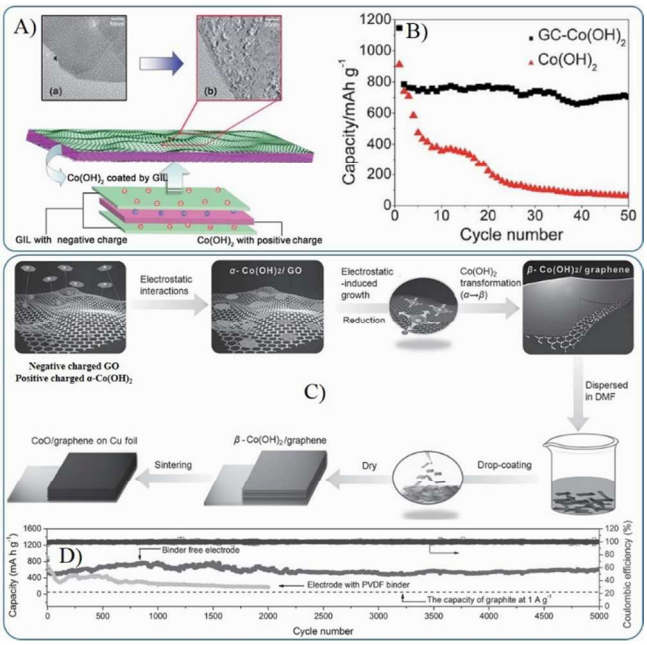

Figure 3. A, Schematic diagram of the fabrication of sandwich structured GC–$Co(OH)_2$ heterostructures driven by the mutual electrostatic interactions between the two species; B, Cyclic performances for GC–$Co(OH)_2$ and pure $Co(OH)_2$[72]. Reproduced from Ref. [72] with permission from The Royal Society of Chemistry. C, Schematic diagram of the fabrication of CoO/graphene hybrid on Cu foil; D, Reversible Li extraction capacity of CoO/graphene hybrid electrode at 1 A g^{-1} for 5000 cycles[73]. Reproduced with permission from Ref. 73 Copyright (2013) WILEY-VCH.

Metal ions from inorganic and/or organic metal salts can also be absorbed on the surface of negatively charged RGO or GO via electrostatic interactions or coordination bonds in RGO or GO suspensions. Starting from the metal ion–GO/RGO dispersions, wet–chemistry strategies, such as *in–situ* chemical deposition, sol–gel processes and hydro–/solvothermal synthesis, are widely used to fabricate a broad range of MOs–G composites. In these strategies, suspended RGO/GO acts as a 2D precursor to form an integrated support network for discrete metal ions, then composites are formed by hydrolysis or *in situ* redox reactions to anchor MOs on the surface of RGO, and further followed by various reducing and annealing processes. Special emphasis is that graphene can suppress the agglomeration of MOs nanoparticles during preparation process.[49] Researches indicated that Co_3O_4 nanoparticles with a size of 5–20 nm were homogeneously anchored on the surface of graphene, while sub–microparticles were obtained without graphene (**Figure 4**).[81] Furthermore, the presence of graphene can also affect the morphology of MOs. Our research indicated 1D Co_3O_4 nanorods were generated instead of aggregated nanoparticles when GO was added to the alcohol–water mixed solvent.[82] Right now, wet chemistry strategies are widely used to fabricate 3D MOs–G composites, which provide simple and practical ways to obtain uniform distribution of MOs nanostructures anchored on graphene with controlled size, morphology and crystallinity.[49]

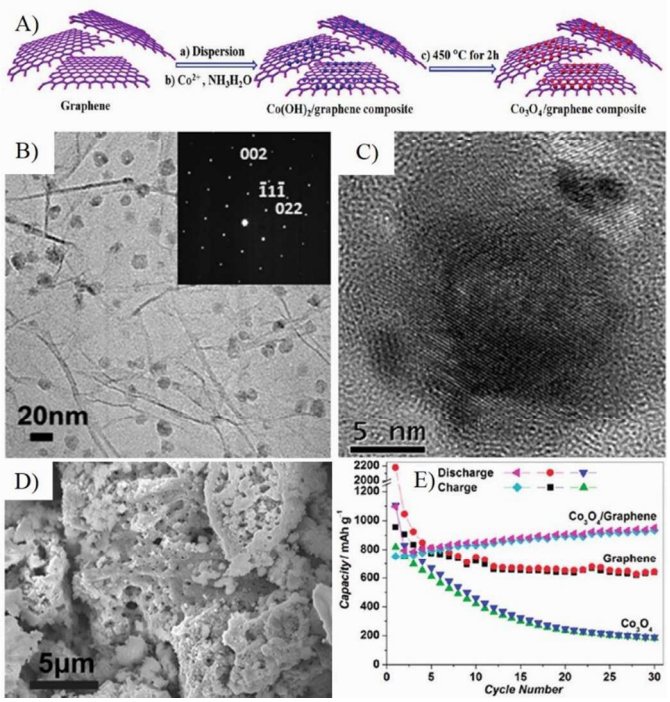

Figure 4 A, Schematic representation of the fabrication process of Co_3O_4/graphene composite. B–C, TEM and HRTEM images of Co_3O_4/graphene composite; the inset in (C) is the SAED pattern of Co_3O_4 NPs with [110] plane in the Co_3O_4/graphene composite, indicative of the well–textured and single–

RSC Advances Accepted Manuscript

This journal is © The Royal Society of Chemistry

crystalline nature of Co_3O_4 NPs. D, SEM image of the as–prepared Co_3O_4, which shows that only micro–sized Co_3O_4 particles can be formed without the presence of graphene sheets. E, Cycling performance for graphene, Co_3O_4, and the Co_3O_4/graphene composite.[81] Reproduced with permission from Ref. 81 Copyright (2010) American Chemical Society.

Surfactants are commonly used in fabricating stable graphene dispersion and synthesizing MOs nanostructures.[62, 83-85] Anionic sulphate could help the thermal reduced graphene dispersing in aqueous solution and facilitate the self–assembly of the *in–situ* grown nanocrystalline TiO_2.[86] The method is further developed to fabricate ordered mesoporous MOs–G nanocomposites, such as SnO_2, NiO or MnO_2–graphene composites.[87] Besides the stabilization of graphene in aqueous/solvent solution, surfactants can also control the size and morphology of MOs in wet chemistry strategy. Co_3O_4–graphene nanocomposites with high loading and highly dispersed Co_3O_4 nanoparticles were fabricated by the co–assembly of polyvinylpyrrolidone (PVP) protected precursors and GO, while Co_3O_4 nanoparticles would agglomerate without surfactant.[88] With the help of the *in–situ* formed dehydroascorbic acid, oxided product of L–ascorbic acid, GNSs decorated with ultra–small Fe_3O_4 nanoparticles were synthesized from Fe^{3+}–GO suspension and L–ascorbic acid via hydrothermal method.[89] SnO_2 nanorods/graphene nanocomposites have been synthesized through a simple ultrasonic combined hydrothermal process with the assistant of mercaptoacetic acid.[90] Moreover, the approach can be extended to produce other MOs nanostructures on the surface of graphene, such as mesoporous spheres,[91-94] nanospindles,[95, 96] nanorods,[97-99] nanowires,[100, 101] nanotubes,[102] nanoplates,[103] nanobelts,[104, 105] nanosheets[106-108] and 3D hierarchical structures.[109, 110]

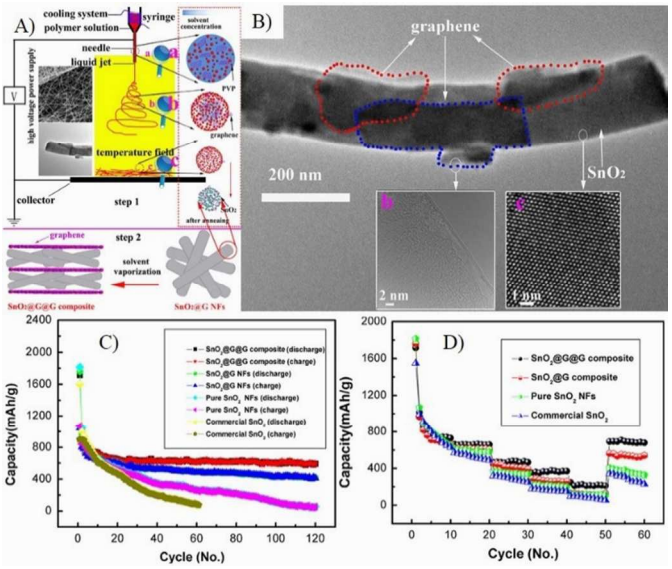

Figure 5. Illustration of synthesis process (A), TEM(B), cyclic(C) and rate (D) performances of SnO_2@G NFs.[135] Reproduced from Ref. 135, Copyright (2014) with permission from Elsevier.

In the wet chemistry strategies, the reduce of GO to RGO or graphene can be carried by many methods, such as metal ions (Fe^{2+}, Sn^{2+}) *in–situ* reduction process,[111-115] chemical reduction process,[89, 116-120] hydro–/solvothermal reduction,[90, 101, 116, 121-126] and thermal reduction.[127-131] Post thermal reduction under inert atmosphere is always introduce to increase the electronic conductivity of composites and further enhance the rate capability of LIBs. Furthermore, proper heat treatment can make the graphene crosslinking and wrapping, resulting a more stable composite structure and leading to good cyclic stability. Based on the wet chemistry strategy, several novel and effective processes have been developed. Considering metal ions–GO/RGO suspension as a sol, MnO–[132] and Fe_3O_4[133]–graphene composites have been prepared by the modified sol–gel method via the solvent evaporation and thermal reduction in sequence. Electrostatic spray deposition,[134] electrostaticinduced spread[73] and electrospun technology[135, 136] were also introduced to synthesize MOs–graphene composites. Binder free electrodes synthesized by these methods always showed good cyclic stability and rate capability because of the well dispersed/wrapped MOs nanomaterials and interconnected high electronic conductive graphene 3D network (**Figure 5**).

Microwave heating technique was successfully applied to synthesize nanomaterials in past years. Magnetite/graphene[137] or Co_3O_4–graphene sheet–on–sheet nanocomposites[138] also have been prepared by the method. However, these obtained composites still need a post thermal reduction process. Pinna et al. invented a one–pot non–aqueous synthesis method of crystalline SnO_2– and Fe_3O_4– based graphene heterostructures in 5–10 minutes by combining the microwave heating and the 'benzyl alcohol route' together, which allowed the selective growth of MOs nanoparticles on the surface of GO. Up to now, microwave based approaches have been utilized to synthesize Fe_2O_3–RGO composites,[139, 140] sheet–like and/or fusiform CuO nanostructures grown on graphene, SnO_2–RGO composites,[141, 142] Mn_3O_4–G composites,[143] Cu_2O@Cu–Graphene composites,[144] MoO_3/graphene film[123] and Zn_2GeO_4/N–doped graphene nanocomposites.[97]

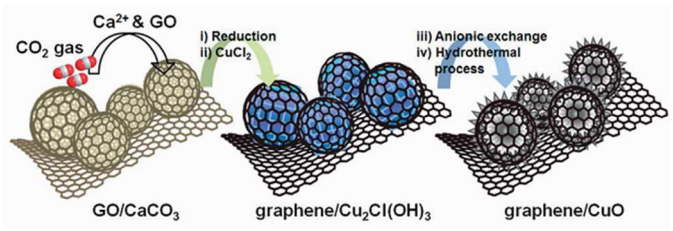

Figure 6. Schematic illustration of sequential steps for the synthesis of graphene/CuO. GO/$CaCO_3$ was prepared by applying CO_2 gas to Ca^{2+} and GO suspension. Graphene/$Cu_2Cl(OH)_3$ was formed by chemical reduction of GO to graphene and transformation of $CaCO_3$ into $Cu_2Cl(OH)_3$. Graphene/CuO was synthesized from graphene/$Cu_2Cl(OH)_3$ by anionic exchange and a hydrothermal process.[145] Reproduced from Ref. 145 with permission from The Royal Society of Chemistry.

Other special technologies also have been developed to prepare MOs–G composites, such as photocatalytic synthesis,[146] coelectrodeposition,[147] atomic layer deposition,[148] supercritical alcohols/CO_2[149-151] and template methods.[145] Especially, the template method is an effective process to

RSC Advances Accepted Manuscript

generate 3D MOs on graphene (**Figure 6**). No matter what methods, the key points in the synthesis of 3D MOs–G composites are 1) generating well dispersed and tightly fixed MOs on graphene, 2) enhancing the electron conductivity of graphene, 3) producing a porous structure to make electrolyte accessible and facilitate the Li^+ diffusion, 4) low cost and environmental friendly.

Table 1 Summary of structures and electrochemical properties of MOs–G composites reported in literatures.

MOs–G[a] Composites	MOs Morphology	Synthesis method	MO content (Wt%)	ICE[b]	Cyclic Performance				Rate Performance		Refs.
					Current density (mA g^{-1})	Initial Capacity (mAh g^{-1})	cycles	Remain Capacity (mAh g^{-1})	Current density (mA g^{-1})	Capacity (mAh g^{-1})	
Graphene composites with 0 D MOs											
Co_3O_4/CoO–G	Nanoparticles	Auto–combustion synthesis	90	76	21	890.4	30	801.3	2100	284	152
Co_3O_4–G	Nanoparticles	PVP assistant reflux	71	–	40	1300	40	860	1000	400	88
Co_3O_4–G	Nanocrystals	Hydrothermal method	76	70.1	400	~900	50	775.2	2000	460	153
Co_3O_4–G	Polyhedral particles	Hydrothermal method	-	~65	50	800	80	885	700	395	122
$CoFe_2O_4$–G	Nanoparticles	Coprecipitation & Thermal reduction	82.3	~71	100	982	50	985	1600	509	154
$CoFe_2O_4$–G	Nanoparticles	Hydrothermal method & Thermal reduction	77.5	69	100	899	70	921.8	1600	446.3	130
CoO–G	Octahedral nanocrystals	Thermal decomposition	40.7	60.30	100	1184	60	1401	8000	~500	155
Cr_2O_3–C[c]–G	Nanoparticles	Hydrothermal method & Thermal reduction	41.9	72.50	106	894.5	100	630	1000	315	131
SnO_2–C–G	Nanoparticles	Evaporation & Thermal reduction	-	65.80	200	656.9	100	633.2	1600	379.5	156
SnO_2–C–G	Nanoparticles	Hydrothermal method	50.3	~51	50	756	150	470			124
CuO–G	Nanoparticles	Spex–milling	90	47.20	0.1 mA cm^{-2}	785.2	45	496.5	6.4 mA cm^{-2}	201	70
$Fe_2Mo_3O_8$–G	Nanoparticles	Hydrolysis & Thermal reduction	91.7	72.40	200	923.5	40	835	3000	574.8	157
Fe_2O_3/SnO_2–G	Nanoparticles	Hydrothermal method–in situ reduction	82	63.30	400	746	100	700	8410	139	158
Fe_2O_3–C–G	Nanoparticles	Evaporation & Thermal reduction	-	–	500	~500	100	504	2000	288.6	156
Fe_2O_3–C–G	Sub-microparticles	Hydrothermal method & Glucose impregnation–pyrolysis process	85	71	200	1097	50	1005			159
Fe_2O_3–G	Nanoparticles	Hydrothermal method	32	~60	100	1000	50	810	2500	280	160
Fe_2O_3–G	Nanoparticles	Spray Drying	86.7	72	100	756	25	870.5	1600	660	161
Fe_2O_3–G	Nanoparticles	Hydrothermal method	68	56.30	200	800	200	852	4000	425	162
Fe_2O_3–G	Microsphere	Hydrothermal method	70	77.20	50	899	50	1206	1000	534	163
Fe_2O_3–G	Nanoparticles	Hydrothermal method & Freeze–drying process	78	69	100	1045	50	995	2000	624	164
Fe_2O_3–G	Nanoparticles	Hydrothermal method	73	~69	100	1095	70	~950	800	~700	165
Fe_2O_3–G	Nanoparticles	Thermal decomposition	68.1	53	100	750	50	900	5000	500	166
Fe_2O_3–G	Nanoparticles	PVP hydrolysis	80	77	200	1107	50	1052	2000	690	167
Fe_3O_4–CNF–G	Nanoparticles	Wet immersion method	41.6	~60	1000	1400	100	1427.5	5000	592	168
Fe_3O_4–G	Nanoparticles	Solution mixing method	78	63.40	500	902	100	892	2000	672	169
Fe_3O_4–G	Nanoparticles	Supercritical CO_2–ethanol	75	73.50	1000	941	100	838	5000	460	151
Fe_3O_4–G	Nanoparticles	Solution mixing & Thermal reduction	-	66.90	100	908.6	50	1082	6000	145	170
Fe_3O_4–G	Nanoparticles	Thermal evaporation & Thermal reduction	78	67.30	200	1443	100	868	1000	539	133
Fe_3O_4–G	Nanoparticles	Microwave assisted "benzyl–alcohol route	58.9	55.70	100	1050			1600	~500	140
Fe_3O_4–G	Nanoparticles	Electrostatic Self–Assembly	55.5	59.90	200	674	100	540	2000	384	76
Fe_3O_4–G	Nanoparticles	Hydrolysis	-	61	92.8	814			4860	282	171
Fe_3O_4–G	Nanoparticles	Hydrothermal method	30	59.20	100	1037	200	1130	1600	648	172
Fe_3O_4–G	Nanoparticles	Hydrothermal method	82.2	65	900	960	133	833	1800	437	89
Fe_3O_4–G–G	Nanospheres	Electrostatic interactions&Hydrothermal method	93.7	~67.3	93	920.3	150	1059	4800	363	75
FeOOH–G	Nanoparticles	Infrared Irradiation	69	67.10	1000	~800	600	767	2000	608	173
G–Co_3O_4–G	Nanoparticles	Hydrothermal method & Mixing method	46.1	~69.5	89	820	50	715.3	892	310	174
GeOx–G	Nanoparticle	Thermal Ge/Sn co–evaporation	70	51.10	325	1047	100	1008	5850	723	175
G–NiO–G	Nanoparticles	Hydrothermal method&Mixing method	44.1	54.90	72	639.4	50	617.6			174
La_2O_3–NiO–G	Nanoparticles	Physical mixing	50	53.00	50	458.6	100	418.2	-	-	176
Mn_3O_4–G	Nanoparticles	Hydrothermal method	64	62.70	200	900	40	800	2000	382	121
$MnFe_2O_4$–G	Nanoparticles	Ultrasonic process	90	60	100	949	50	1017	12000	315	67
MnO_2–G	Nanoparticles	Hydrothermal method	-	64	100	781.5	50	750	1000	465.2	177
MoO_2–G	Nanoparticles	In situ reduction process	93.5	75.40	0.2 C	1067.7	100	950	10 C	411.7	178

RSC Advances Accepted Manuscript

This journal is © The Royal Society of Chemistry

MoO_3–G	Nanoparticles	Solution mixing method	73.96	–	800	961.5	50	711			179
$NiFe_2O_4$–G	Nanoparticles	Coprecipitation & Thermal reduction	87.9	~72	100	1225	50	1005	1600	758	154
NiO–G	Nanoparticles	Supercritical CO_2–ethanol	68.5	65.10	500	629	100	741	2000	350	150
NiO–G	Nanoparticles	Electrochemical	87.3	59.30	359	754	50	586	1440	~500	180
SnO_2–C–G	Nanoparticles	Hydrothermal method & Thermal reduction	51.4	54	100	1115	100	~1000	1000	499	128
SnO_2–C–G	Nanoparticle	Hydrothermal method & Carbonization process	74.5	60	100	1058	80	703	1000	443	181
SnO_2–C–G	Nanoparticles	Evaporation & Thermal reduction	-	65.80	200	656.9	100	633.2	1600	379.5	156
SnO_2–C–G	Nanoparticles	Hydrothermal method	50.3	~51	50	756	150	470			124
SnO_2–G	Nanoparticles	Refluxed & cross–linking reaction	81.8	–	100	1282	50	521	2000	334	111
SnO_2–G	Nanoparticles	Microwave & Thermal reduction	85	54.40	100	1329.4	20	618			129
SnO_2–G	Nanocrystals	*In–situ* Sn^{2+} reduction	72	54	100	1017	50	610	2000	372	182
SnO_2–G	Nanoparticles	Polyol reduction	30	73	90	1890	100	1220	1000	602	183
SnO_2–G	Quantum Dots	Hydrothermal method	50	~43	200	800	200	720	2000	400	184
SnO_2–G	Nanoparticles	Wet chemical method	80	96.4	1000	1923.5	40	1545.7			112
SnO_2–G	Nanoparticle	Unzipping CNT&ultrasonication	80	74	100	1129	50	825	2000	580	185
SnO_2–G	Nanoparticle	Sn^{2+} in situ reduction& self–assembly	-	~39	100	~900	60	602	1000	200	186
SnO_2–G	Nanoparticles	Template	89	~51	100	878	40	503			187
SnO_2–G	Nanoparticle	Hydrothermal method assembly	53	56	100	1211	70	824	500	621	188
SnO_2–G	Nanoparticle	Sn^{2+} oxidation–reduction reaction	68.1	45.60	100	1254.6	30	985.5			189
SnO_2–G	Nanoparticle	Sn^{2+} Ultrasonic & Oxidation–reduction reaction	38.4	~62	100	627	50	535			190
SnO_2–G	Nanocrystals	Freeze–drying & Vapor reduction process	70	61.30	500	1144	500	1346	20000	417	191
SnO_2–GO–G	Nanoparticles	Electrostatic interactions	72.9	55.90	100	~1100	200	872	2000	519	80
SnO_2–In_2O_3–G	Nanocrystals	Solvothermal	90.37	57.20	60	907	50	551	600	393	192
SnO_2–In_2O_3–G	Nanocrystals	Hydrolysis–chemical reduction & thermal reduction	50	66.40	75	770	30	570	900	504	193
SnO_x–CNF@G–G	Nanoparticles	Electrospinning calcination & Mixing method	72	62.3	70	838	180	504	700	300	136
$SnWO_4$–G	Nanoparticle	Hydrothermal method	80	55	50	934	20	500			194
TiO_2–G	Nanocrystals	Hydrothermal method	93.7	69.30	200	171	100	137	4000	69	195
TiO_2–G	Nanoparticles	In–situ Hydrothermal methodgrowth	65	58.50	200	237	100	157	2000	122	196
TiO_2–G	Nanoparticles	Hydrolysis &Hydrothermal method	83		0.2C	226			20C	97	197
TiO_2–G	Nanoparticle	Gas/liquid interface reaction	-	–	1000	~150	80	136	5000	109	198
TiO_2–G	Nanoparticles	Atomic layer deposition	54.7		2000	100	500	95			199
TiO_2–SnO_2–G	Nanoparticles	Solvothermal & Hydrothermal method	90	49	50	954	50	537	1000	250	200
V_2O_5–G	Quantum dots	Two–step solution phase synthesis	93.55	97.20	100	280	100	212	1000	118	201
V_2O_5–G	Nanoparticles	Hydrothermal method	92	–	20	235	100	171			202
Zn_2SnO_4–G	Nanocrystals	Hydrothermal method	82.6	54	200	911	50	688	1600	439	203
$ZnFe_2O_4$–G	Nanoparticles	Hydrothermal method	-	68.70	100	945	50	956	1000	~600	204
ZnO–G	Quantum dots	Atomic layer deposition	68	~50	100	700	100	540	1000	400	205
$ZnWO_4$–G	Nanoparticles	Sol–gel method	93	68	50	695	20	585	200	440	206
		Graphene composites with 1D MOs									
$CuGeO_3$–G	Nanowires	Nanowires	81.2	45.5	100	1157	130	780	2000	550	207
Fe_3O_4–G	Nanospindles	Hydrothermal method	-	–	100	745	200	558	–	–	95
Fe_3O_4–G	Hollow nanospindles	Vacuum Filtration and thermal reduction	70.3	66.7	200	~1000	50	940	2000	420	208
Fe_3O_4–G	Nanorods	In–situ growth	75	60.2	928	912	100	867	4640	569	209
GeO_2–G	Microtubes	Strain–driven method	88.6	33	110	856	100	919	2200	571	210
MnO_2–G	Nanowires	Hydrothermal method route	85	–	60	1150	30	890	12000	~600	101
MnO_2–G	Nanorods	Solution mixed & Thermal annealing method	91	70.8	30.8	170.6	100	158.3	–	–	211
Ni–doped MnO_2 –G	Nanowires	Electrostatic interactions	70	95	286	~170	40	122	–	–	212
SnO_2@G@G–G	Nanowires	Electrospinning &Solution mixed method	72	61.6	80	1050	180	591.9	4000	212.8	135, 213
SnO_2–C–G	Nanorod	Seed assisted Hydrothermal method growth & Nanocarbon coating	63	70	100	1285	150	1419	3000	540	214
SnO_2–G	Nanorods	Ultrasonic & Hydrothermal method	67	~60	200	1153	100	1107	2000	583.3	90
TiO_2–G	Nanotube	Hydrothermal method	-	–	100	334	50	255	8000	80	102
TiO_2–G	Nanowires	Hydrothermal method	90.4	–	150	~200	30	~160	–	–	215
TiO_2–G	Nanotubes	Hydrothermal method	95.91	98.9	150	~210	30	278	1500	114	216
WO_3–G	Nanowires	Hydrothermal method	92.1	67.4	100	622	100	656	290	800	100

RSC Advances Accepted Manuscript

Zn_2GeO_4/G–G	Nanorods	Ion–exchange method	87.9	>60	100	873	90	803	3200	522	217
Zn_2GeO_4–G	Nanorods	Hydrothermal method & Microwave process	72.2	~60	100	873	100	1044	3200	678	97
Zn_2GeO_4–G	Hollow nanorods	Hydrothermal method	-	–	100	–	20	900	–	–	218
Graphene composites with 2D MOs											
CoO–G (binder free)	Nanosheets	Electrostatic induced spread	87	71.60	500	678	150	640	1000	604	73
CuO–G–G	Nanosheets	Vacuum filtration & Hydrothermal method reduction	-	91.60	67	782.3	50	736.8			219
Fe_2O_3–CNT–g–G	Nanoring	Chemical vapor deposition	-	~51	74.4	984	100	812	3720	534	220
Fe_2O_3–G	Hexagonal Nanoplatelets	Surfactant assistant limited growth	53		0.2 C	1370	150	1100	5 C	631	221
Fe_2O_3–G	Nanodisk	Hydrothermal method	75.6	71.60	200	1088	50	931	10000	337	127
MoO_3 –G	Nanobelts	Hydrothermal method	-	–	500	289	200	174	1000	238	105
MoO_3–G	Nanobelt	Microwave Hydrothermal method	70	59	100	291	100	172	2000	151	123
SnO_2	Nanosheets	Hydrothermal method	87	71.40	100	975	100	451			222
TiO_2/graphene sandwich paper–G	Nanosheets	In situ Hydrothermal method	82	–	1680	~150	100	147	8500	120	223
TiO_2/SnO_2–G	Hybrid nanosheets	Stepwise growth	95	49	160	841	300	600	4000	300	224
TiO_2@Co_3O_4–G	Coaxial nanobelt arrays	Electrostatic self–assembly	51.1	51	100	364	60	437	800	204	77
TiO_2–G	Nanosheets	Hydrothermal method	75.12	–	1 C	232	100	189	10 C	150	107
TiO_2–G	Nanoplatelets	Solvothermal	78	92	1 C	404	100	350	10 C	165	108
TiO_2–G	Nanobelts	Hydrothermal method	86	82	150	746	100	430	3000	210	104
V_2O_5–G	Nanosheets	Solvothermal	95	89	600	262	160	102	3000	138	225
VO_2–G	Ribbons	Hydrothermal method & Chemical reduction process	84	–	190C	204	1000	~190			117
VO_2–G	Nanosheet	Hydrothermal method	69	–	50	418	50	251	5000	102	226
Zn_2SiO_4–C–G	Layered structure	Hydrothermal method & Vaporization	80	47	50	738	50	778	1000	277	119
Graphene composites with 3D MOs											
Co_3O_4–G	Mesoporous hollow sphere	Solvothermal & Immersed methods	76.2	69.30	1000	~900	200	~700	5000	259	94
Co_3O_4–G paper–G	Porous fibers	Electrostatic Self–Assembly	78.3	71.60	100	1005.7	40	840	100	295	79
Cu_2O@Cu–G	Porous nanospheres	Microwave	85.2	–	50	734	50	842	2000	410	144
Fe_2O_3–G	Porous nanocages	Template method	-	76	200	1239	50	864	5000	587	227
Fe_3O_4/G–G	Porous Nanorods	In situ–growth & Hydrogen plasma treatment	79	77.50	500	845	100	890	3000	520	228
Fe_3O_4/G–G	Interconnected nanoparticles	Template synthesis	74	63.40	500	965	100	1124	10000	506	229
Fe_3O_4–C–G	Mesoporous carbon supported	Template synthesis & Heterocoagulation method	62.4	63.40	92.4	845	100	660	924	380	230
In_2O_3/G–G	Mesoporous	Template synthesis & Heterocoagulation method	87.4	60.80	58	804.5	100	480	580	290	231
$Mn_{0.5}Co_{0.5}Fe_2O_4$–G	Mesoporous nanospheres	Solvothermal method	97.9	59.10	200	846.2	200	886.1	5000	266.3	93
NiO–C–G	Mesoporous carbon supported	Template synthesis & Heterocoagulation method	51.8	61.80	71.8	~820	100	~570	718	~310	230
SnO_2–G	Mesoporous	Electrostatic interactions	-	–	78	~780	50	~460			118
SnO_2–G	Mesoporous	Solvothermal method	79.5	69.40	78	1107	50	847.5	780	621.5	91
SnO_2–G	Porous Nanospheres	Electrostatic interaction	95	43.40	200	750	50	517	1000	423	232
TiO_2–G	Mesoporous nanospheres	Hydrothermal method & Freeze–drying	89	69.70	0.5C	219	100	197	20C	124	92
Zn_2SnO_4–G	Hollow box	Chemical etching & Heat–process	65	69	300	1121.2	60	753	2000	345	233

[a] G: graphene; [b] ICE: initial columbic efficiency; [c] C: carbon.

3 3D MOs–G composites in LIBs

MOs in MOs–G composites are mainly in 0D morphology in the beginning studies, such as nanoparticles[65, 86] and nanocubes[234]. These nanoparticles usually suffer from the aggregation problems even in graphene composites and could be easily peeling off from the surface of graphene due to the weak contact between nanoparticles and graphene during cycling process, resulting in the fast fading of electrode capacity. Composites in wrapped, encapsulated, sandwich–like and layered models can show higher cyclic capability than that of other models. But the rate capability of these composites is usually limited by the diffusion of lithium ions because Li^+ ions cannot pass through the microsized planar GNSs. If the size of

RSC Advances Accepted Manuscript

 This journal is © The Royal Society of Chemistry

nanoparticles is not large enough, pores between GNSs will be too small to access the electrolyte and is harmful for the lithium diffusion. It is important to investigate the size effects of 0D nanoparticles and their dispersion on GNSs to improve the electrochemical performances. These problems also can be solved well by the graphene composites consisted with 1D, 2D or 3D MOs materials, which have at least one dimension in micro or sub–micro size. In this situation, MOs with 1D, 2D and 3D structures can afford more sites to connect with graphene and create many meso- or macropores to make electrolyte accessible, which can further enhance the long term stability and rate capability of LIBs. Furthermore, holey GNSs and stable 3D graphene structures can facilitate the diffusion of lithium ions and increase the rate capability. Thus, the morphology and size of MOs or graphene in composites play important roles on the electrochemical performances of LIBs.

3.1 Morphologies of MOs in composites

The assembling type, pore size/structure, surface area and overall dimensions of 3D MOs–G composites are greatly affected by the morphology and size of MOs. And these properties of 3D MOs–G composites will affect the stability of the hierarchical structure, the access of electrolytes, the diffusion of lithium ions, and further affect the electrochemical performances of LIBs.

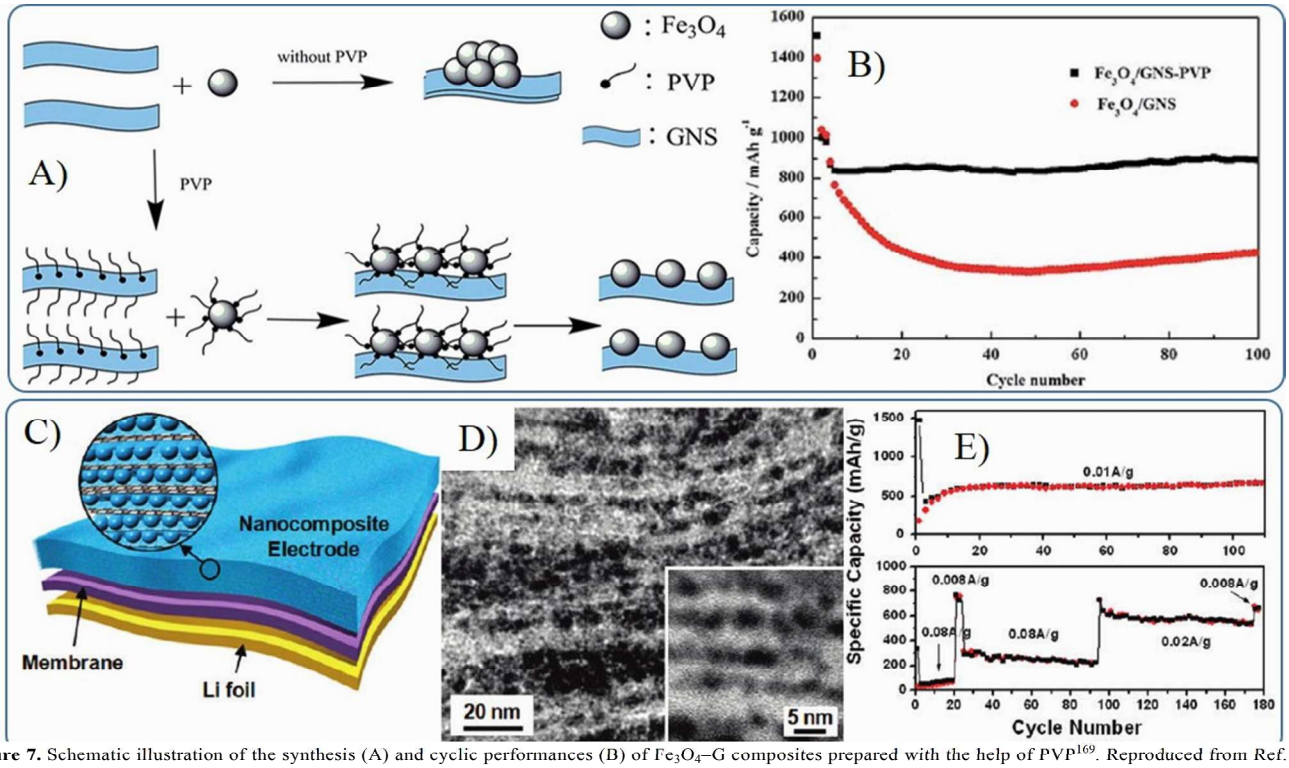

Figure 7. Schematic illustration of the synthesis (A) and cyclic performances (B) of Fe_3O_4–G composites prepared with the help of PVP[169]. Reproduced from Ref. 169 with permission from The Royal Society of Chemistry. Li–ion battery configuration (C), cross–sectional TEM images (D) and cyclic performances (F) of freestanding SnO_2–G nanocomposite film as anode.[87] Reproduced with permission from Ref. 87 Copyright (2010) American Chemical Society.

3.1.1 Graphene composites with 0D MOs

0D nanostructures, including quantum dots, nanoparticles, nanospheres or nanopolyhedra, are point structures with all dimensions in nanoscale, which are also the simplest and easily obtained nanostructures. In the early studying stage of 3D MOs–G composites of LIBs, SnO_2 nanoparticles, [65] TiO_2 nanoparticles [86] and Cu_2O nanocubes[234] were widely studied. Though many other kinds of MOs have been developed for LIBs, most of MOs used in the 3D MOs–G composites are still in 0D nanostructure up to 2013 (Table 1). It is accepted well that the decrease of particle size of MOs can ensure the reversibility of lithium intercalation, increase the rate of lithium insertion/removal, enhance electron transport within particles, and modify the chemical potentials for lithium ions and electrons, etc. Additionally, the graphene in the composites can shorten the migration distance of electrons from MOs to conductive substrate. Thus, the above synergy effects can lead to a high reversible capacity of LIBs. For example, the SnO_2/graphene composite in mixed model showed a reversible capacity of 810 mAh g^{-1}, even higher than the theoretical capacity of SnO_2 (782 mAh g^{-1}).[65] However, only 570 mAh g^{-1} of charge capacity of the composite was kept after 30 cycles. In this case, MOs nanoparticles in the graphene composites in anchored, sandwich–like or mixed model usually suffer from aggregation and can be easily peeled off from the surface of graphene due to the weak contacts between nanoparticles and graphene during cycling process.

To overcome these problems, surfactants can be induced to prevent the aggregation of MOs in graphene. Cai et al. found the presence of PVP could help the dispersion of Fe_3O_4

RSC Advances Accepted Manuscript

nanoparticles on graphene and result a stable capacity of 892 mAh g^{-1} after 100 cycles, compared with that of 430 mAh g^{-1} without PVP (**Figure 7**A–B).[169] Building strong interactions between MOs and graphene is also a good choice to prevent the aggregation of MOs nanomaterials and improve the stability and conductivity of composites, which will be further discussed in following part. Composites in wrapped, encapsulated or layered model usually show higher cyclic stability than that of other models. For instance, the free–standing flexible nanocomposite films produced from layered graphene with 4 nm nanocrystals show no significant fading over 100 charge/discharge cycles (**Figure 7**C–D).[87] However, the composites in wrapped and encapsulated models will suffer from similar lithium ions diffusion problems because lithium cannot effectively pass through the 2D structure of graphene, which will further affect the rate capability. Thus small pore size in composites in layered model (depend on the size of nanoparticles) is harmful for the electrolyte wetting and lithium diffusion, especially leading to an active process in initial several cycles and limiting rate capability. That is why these films only remain a capacity of 225 mAh g^{-1} at 0.02 A g^{-1}, compared to 760 mAh g^{-1} at 0.008 A g^{-1}.[87] Thus, the structure model, graphene structure, dispersion and stability of MOs nanomaterials on the surface of graphene should be considered at the same time to fabricate 0D MOs based graphene composites with high electrochemical lithium storage performances.

3.1.2 Graphene composites with 1D MOs

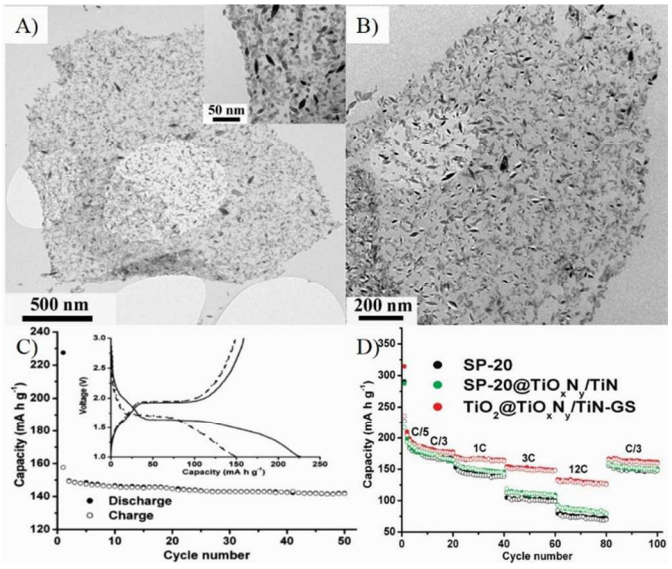

Figure 8. A), a typical TEM image of a TiO_2 nanospindles/graphene oxide nanocomposite (Inset is a close–up view); B), a TEM image of aTiO_2@TiO_xN_y/TiN–G nanocomposite after annealing in NH_3. C), cycling performance of the electrode made of SP–20 at a rate of 1C (voltage profiles). D), cycling specific capacity profiles of SP–20, SP–20@TiO_xN_y/TiN, and TiO_2@TiO_xN_y/TiN–G nanocomposite at different charge/discharge rates.[235] Reproduced with permission from Ref. 235 Copyright (2010) American Chemical Society.

In the last decades, one–dimension (1D) nanostructures, such as nanowires, nanotubes and nanorods, have attracted considerable attention due to their potential magnetic, optical, electrical and catalytic properties.[236, 237] To be considered as the smallest dimension nanomaterials, 1D MOs nanomaterials are particularly interesting in LIBs, owing to save for the large surface to volume ratio, their vertical transportations of ions and electrons and apt accommodation of lithiation induced stresses.[235, 238] On the other hand, 1D nanostructures are line contact with substrate, compared with point contact of 0D materials, so it is reasonable to believe that the graphene composites with 1D MOs nanomaterials would possess high electronchemical performances in LIBs. For example, Qiu et al successfully synthesized surface–nitridated TiO_2 nanospindles–graphene nanocomposites by an *in–situ* alkyl amines assistant hydrothermal process, and they found the obtained composites showed enhanced cyclic stability and rate capability due to the ordered dispersion of dense ultrafine TiO_2 nanospindles on GNSs and the thin TiN/TiO_xN_y layer on TiO_2 nanospindles (**Figure 8**).[235]

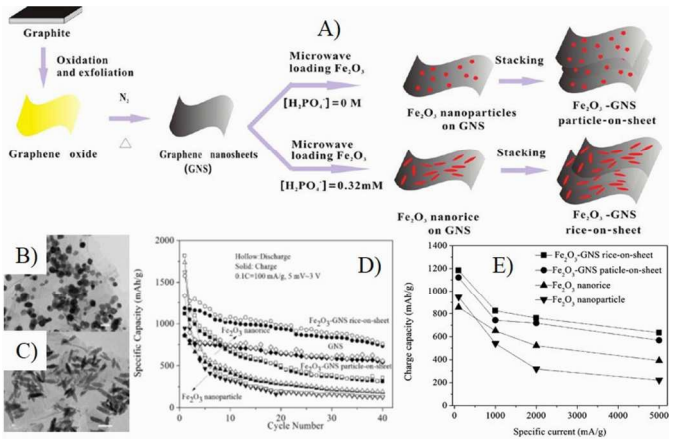

Figure 9. Schematic illustration of the growth process (A), TEM images (C–D), cyclic (D) and rate (E) performances of Fe_2O_3–GNS particle–on–sheet and rice–on–sheet composites. [239] Reproduced with permission from Ref. 239 Copyright (2011) American Chemical Society.

The morphologies of MOs also affect the electron conductivity of composites. Graphene composites with Fe_2O_3 nanorices (~200 nm in length and ~40 nm in diameters) and cube–like nanoparticle (50–100 nm) were controlled synthesized by a microwave–assisted hydrothermal process.[239] The electrical conductivities of Fe_2O_3 nanoparticles, Fe_2O_3–GNS particle–on–sheet and Fe_2O_3–GNS rice–on–sheet are 2.8×10^{-5} S/cm, 0.038 S/cm and 0.049 S/cm, respectively, indicating that the composite with 1D Fe_2O_3 nanoparticles has highest electron conductivity.[239] As shown in **Figure 9**, Fe_2O_3–GNS rice–on–sheet shows superior electrochemical performances compared with that of particle–on–sheet at both common and high current rates, because the special 1D Fe_2O_3 nanorice can not only increase the electron conductivity, but also facilitate the lithium diffusion rate for their high surface–to–volume ratio. And heavy agglomeration of Fe_2O_3 nanoparticles are more inclined to occur compared with that of Fe_2O_3 nanorice.[239] Then graphene–Fe_2O_3 nanocomposites with different loading of Fe_2O_3 nanospindles were prepared by the

RSC Advances Accepted Manuscript

 This journal is © The Royal Society of Chemistry

one–step solvothermal method,[96] and the obtained composites showed a higher electron conductivity of 0.10–0.13 S/cm (depend on the content of graphene), which further lead to an improved rate capability compared with Fe_2O_3–GNS rice–on–sheet used as anodes in LIBs.[96, 239]

Co_3O_4 nanorods/GNS nanocomposites were synthesized via a one–pot solvothermal method by completing the reduction of GO and the growth of Co_3O_4 nanorods simultaneously.[82] The obtained Co_3O_4 nanorods–GNS nanocomposites exhibited approximate 1310 mAh g^{-1} and 1090 mAh g^{-1} of capacity at 0.1 A g^{-1} and 1 A g^{-1} after 40 cycles, respectively.[82] The improvement of electrochemical performances of Co_3O_4 nanorods–GNS nanocomposites can be attributed to the unique structures and properties of GNS and Co_3O_4 nanorods, which can provide an excellent ion diffusion and electronic conduction pathway, and further lead to a superior electrochemical performance. Recently, we further developed a small molecule assistant hydrothermal method to directly grow SnO_2 nanorods on GNSs, which were further assembled to a layered structure.[90] The as–prepared nanocomposites kept a reversible capacity of 1107 mAh g^{-1} within 100 cycles at a current density of 0.2 A g^{-1}, retaining 96.2% of the initial value. The capacity, stability and rate capability of the layered structure are much higher than that of single layer monodispersed SnO_2 nanorods growth on GNSs[98, 99], which may be attributed to the additional stability and electron conductivity derived from the interlayered/interconnected graphene in the layered model of composite. The concept is further supported by the high electrochemical performances of Free–standing layer–by–layer assembled graphene-MnO_2 nanotube thin hybrid films prepared by an ultrafiltration technique.[240] In all, the unique physiochemical properties of 1D MOs in tandem with the synergistic effects of graphene composites promise a high electrochemical performances in LIBs, which will be greatly affected by the size of 1D MOs, graphene quality and the structure models of composites.

3.1.3 Graphene composites with 2D MOs

Unique 2D nanosheets have been extensively studied because they can enhance the intrinsic properties of their bulk counterparts as well as generate new promising properties. 2D nanostructures can offer a face to face contact model, which can utilize nearly half of the surface area and result in much more strong interactions than that of 0D and 1D nanostructures. Thus, 2D nanostructures would show better mechanical stability and enhanced charge exchange properties between MOs and substrates, and the graphene composites with 2D MOs nanomaterials are expected to have unique electrochemical performances used as electrode materials in LIBs. The fabricated $Co(OH)_2$ nanoplates–GNS composites by hydrothermal process open the door of the application of graphene composites in LIBs, which show a capacity of 910 mAh g^{-1} after 30 cycles, compared with the initial reversible capacity of 1120 mAh g^{-1} at 200 mA g^{-1}.[242]

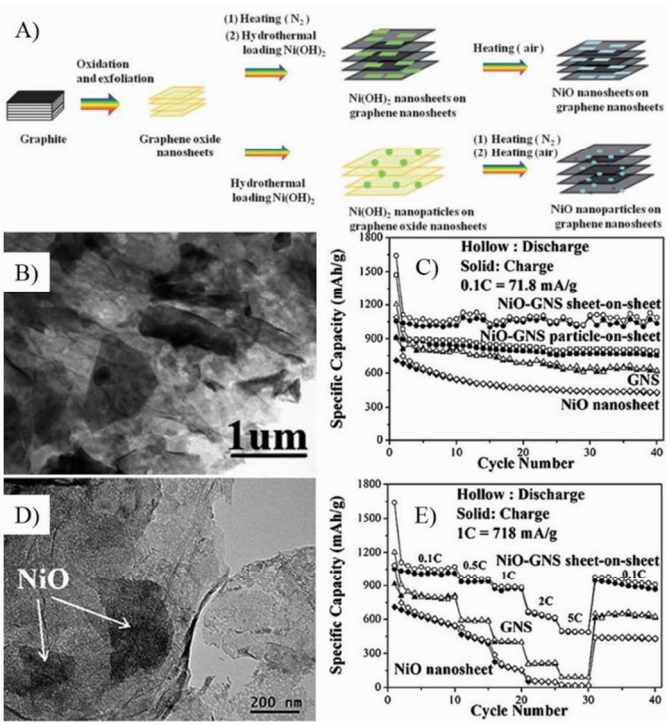

Figure 10.A), Schematic illustration of the growth process of NiO–GNS sheet–on–sheet and nanoparticle–on–sheet composites; B), TEM image of NiO–GNS sheet–on–sheet composite; C), cycling performances at 0.1 C of various anode materials; D), TEM image of NiO–GNS sheet–on–sheet anode after 40 cycles, E), cycling performances at stepwise increased current rates.[241] Reproduced from Ref. 241 with permission from The Royal Society of Chemistry.

In these graphene composites with 2D MOs nanostructures, the lithium diffusion within 2D MOs may decide their lithium storage performances, especially the high rate performances. Wang et al. synthesized $Co(OH)_2$–graphene sheet–on–sheet composites by a single–mode microwave irradiation method, and layered Co_3O_4–GNS sheet–on–sheet nanocomposites were obtained after being further post thermally treated under N_2 to improve the quality and electron conductivity of graphene.[68, 81, 138, 204, 243] The unique structure shows good stability of electrochemical properties after 30 cycles. In the composite, plenty of pores in composite and Co_3O_4 nanosheets can accelerate the phase transition, restrain the crumbling and cracking of electrode, and further lead to superior cycling stability. Furthermore, the porous structure of Co_3O_4 nanosheets is readily accessible for electrolyte, facilitating the transportation of Li^+ ions from liquid to active surface of Co_3O_4 and shorting the transportation length for both lithium ions and electrons.[138] Thus, the rate performances of composites are significantly improved, and a capacity of 931 mAh g^{-1} is obtained at a current density of 4450 mA g^{-1}, which is larger than the theoretical capacity of Co_3O_4 (890 mAh g^{-1}). While only half of the capacity for Co_3O_4–graphene nanoparticle–on–sheet is obtained at the same conditions.[138] Then they prepared NiO–graphene sheet–on–sheet and nanoparticle–on–sheet nanostructures (**Figure 11**), the stable sheet–on–sheet structures showed highly stable reversible capacities (1056–1031 mAh g^{-1} in 40 cycles at 71.8 mA g^{-1}) and good rate capabilities (492

RSC Advances Accepted Manuscript

mAh g^{-1} at 3590 mA g^{-1}) than those of NiO nanosheets, GNSs, and NiO–graphene nanoparticle–on–sheet.[241] Both the above results and other researches[106, 244, 245] indicate the electrochemical performances of graphene composites with 2D structures are better than ones of 0D structures, derived from the stable and porous 2D structure.

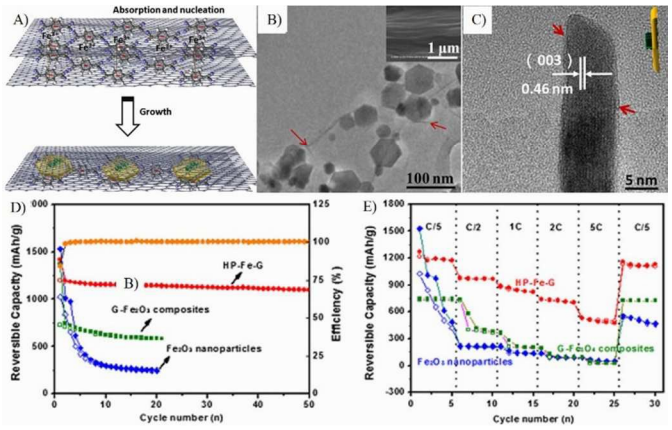

Figure 11. Schematic illustration of the formation process (A), TEM imgages (B–C), cyclic (A) and rate (B) performances of a–Fe_2O_3 hexagonal nanoplatelets sandwiched between graphene sheets (HP–Fe–G).[221] Reproduced from Ref. 221, Copyright (2013) with permission from Elsevier.

Besides the porous structure, ultrathin nanosheets can also reduce the diffusion distance of Li ions, so the graphene composites with ultrathin Fe_2O_3 nanosheets (**Figure 11**)[221] and VO_2 ribbons[117] show remarkable stability and rate capability as porous 2D structures. These graphene composites with special 2D MOs nanostructures show following inspirations: (1) face to face contact model can enhance the electron contact, good mechanical and electrochemical stability of composites; (2) the enhanced electron contact with interconnected graphene network can lead to high electron conductivity; (3) ultrathin and porous 2D nanostructures can provide numerous channels for the access of electrolyte and facilitate the rapid diffusion of lithium ions.

3.1.4 Graphene composites with 3D MOs

3D hierarchical materials built by nanosized unites have both the advantages of nanomaterials and bulk materials. Furthermore, they can overcome the aggregation and/or separation of nanomaterials. The benefits of 3D hierarchical structures in LIBs have been summarized in previous section (2.1). But the main problem of pure 3D hierarchical MOs is their poor electron conductivity, which can be solved well by compositing with graphene. In 2010, urchin–like CuO/graphene composites synthesized via a wet chemistry strategy showed the improved cyclic stability and rate capability compared with urchin–like CuO particles.[109] The urchin–like SnO_2/graphene nanocomposites prepared via electrostatic attraction assisted co–assembly process could also significantly increase the capacity and cyclic stability of tin oxides.[246] Up to now, several graphene composites with 3D hierarchical structures have been fabricated by combining the reduction of GO and the formation of hollow/porous MOs through one pot wet–chemistry process, such as porous V_2O_5 spheres,[247] hollow Fe_2O_3 spheres,[248] hollow porous Fe_3O_4 beads,[249] porous TiO_2 nanospheres,[250] mesoporous anatase TiO_2 nanospheres,[251] mesoporous SnO_2,[91] mesoporous $Mn_{0.5}Co_{0.5}Fe_2O_4$ nanospheres,[93] Fe_3O_4 nanorods,[228] and etc. These obtained composites usually exhibited the improved electrochemical performances in LIBs.

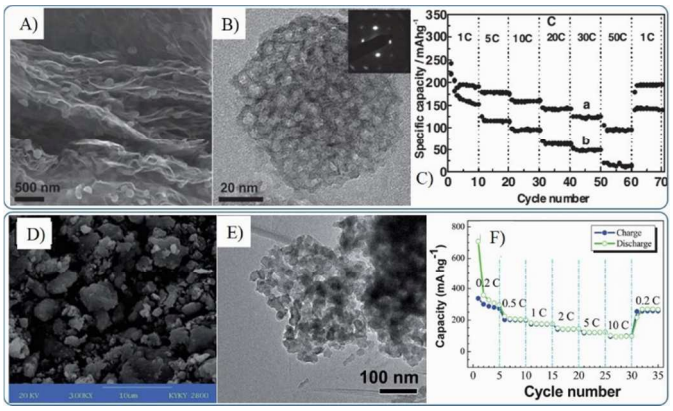

Figure 12. SEM (A,D), TEM (B,E) images and rate capability (C,F) of mesoporous anatase TiO_2 nanospheres–Graphene composites(A–C)[251]and porous TiO_2 nanospheres–Graphene composites (D–E)[250]. A-C, Reproduced with permission from Ref. 251 Copyright (2011) WILEY-VCH. D-E, reproduced from Ref. 250with permission from The Royal Society of Chemistry.

Though the one–pot synthesis method of graphene composites with 3D MOs is facile and easy, it is lack of universality. Recently, the co–assembly of graphene and 3D MOs has been widely developed to fabricate the composites of graphene and 3D MOs, in which mesoporous MOs were pre–synthesized by template methods[118, 230, 231, 252, 253] or one pot processes.[66, 94] Furthermore, template[145, 227, 229] and chemical etching[233] methods were also used directly to prepare graphene nanocomposites with 3D MOs. The electrochemical performances of the obtained graphene and 3D MOs composites are decided by the primary particle size, pore structure and post reduction process. Moreover the lithium storage performances, especially the high rate performance, are strongly depend on the size of building units. As shown in **Figure 12**, graphene–mesoporous TiO_2 nanospheres composites with the primary particles of 4 nm in size show a capacity of 97 mAh g^{-1} at 8.4 A g^{-1}, while the nanocomposites with the primary particles of 20–30 nm in size keep a capacity of 97.7 mAh g^{-1} at 1.68 A g^{-1}.[250, 251]

3.2 Morphologies of graphene

Due to the 2D nature of graphene, Li^+ ions are difficult to directly transmit through GNSs. Furthermore, the conductivity between individual graphene nanosheet also affects the rate performances of nanocomposites. Thus the morphologies, size and structures of graphene in composites are also very important for LIBs. To overcome the above problems, 3D graphene structures (free–standing graphene and graphene oxide sponges) were synthesized firstly by special drying process, in which the strong interactions of graphene oxide in water played an important role. After being loaded by MOs

RSC Advances Accepted Manuscript

 This journal is © The Royal Society of Chemistry

nanomaterials and post reduced, the obtained graphene composites will show outstanding electrochemical performances.[92, 227, 255] For example, magnetite modified GNSs kept a capacity of 450–500 mAh g^{-1} at 5 A g^{-1}

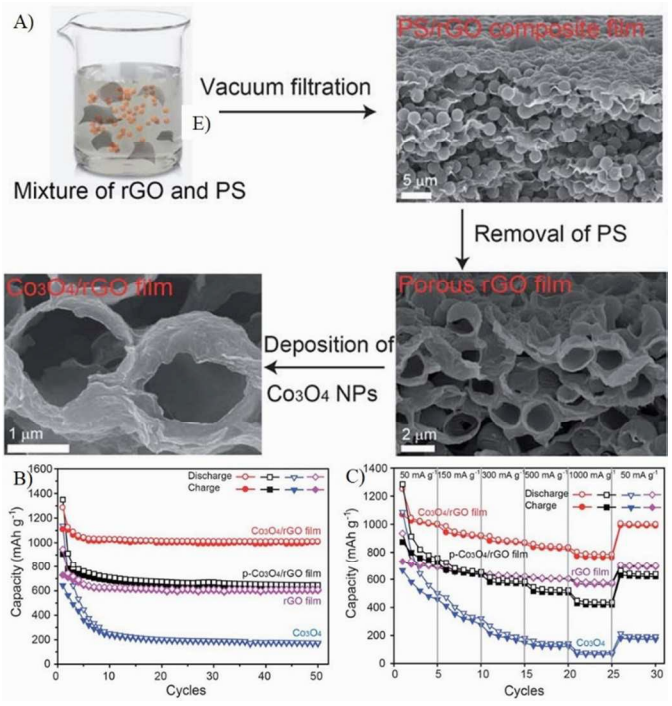

Figure 13. Schematic illustration of the formation process (A), cyclic (B) and rate (C) performances of Co3O4/rGO films. [254] Reproduced from Ref. 254 with permission from The Royal Society of Chemistry.

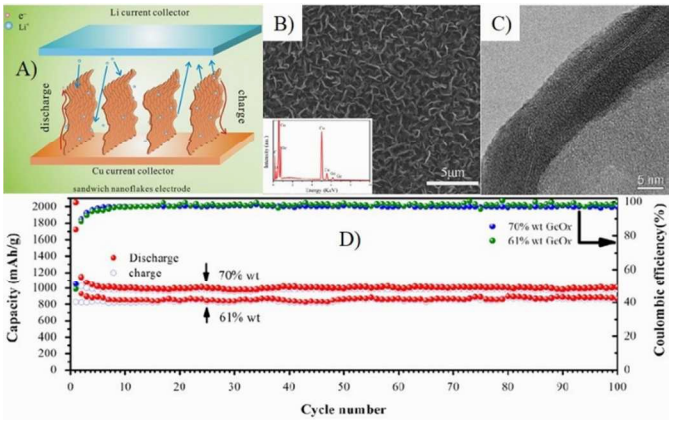

Figure 14. Scheme of the lithium ion diffusion mechanism in VAG@GeO_x sandwich nanoflakes based electrode (A), SEM (B) and TEM (C) image of the flake edge, clearly shows the sandwich structure of VAG@GeO_x composites. D, cycling performance of the electrodes with different load, 70 wt% and 61 wt%, both were tested at the rate of C/3.[175] Reproduced from Ref. 175 Copyright (2013) with permission from Elsevier.

during 1000 cycles.[256] Co_3O_4 nanoparticles deposited onto porous graphene showed a good cycling performance with 90.6% retention of the original capacity after 50 cycles and enhanced rate capability with 71% capacity retention at 1 A g^{-1}, compared with the capacity at 0.05 A g^{-1}(**Figure 13**).[254] Fe_2O_3 coated three–dimensional (3D) graphene composites kept a capacity of 864 mAh g^{-1} at 0.2 A g^{-1} and 587 mAh g^{-1} at 5 A g^{-1} after 50 cycles.[227] These 3D frameworks with interconnected porous structures can effectively reduce the diffusion length of electrons and Li^+ ions, and the cross–linked graphene network can provide multidimensional pathways to facilitate the transport of electrons in the bulk electrode.

Recently, amorphous GeO_x coated vertically aligned GNS composites were synthesized by microwave plasma enhanced chemical vapor deposition system combined with chemical vapor deposition process,[175] in which GNSs formed a fast electron transport channel due to its superior electron conductivity and the vertically aligned sandwich nanoflakes. The unified orientation of GNSs could reduce effectively the vertical lithium diffusion and offer a short pathway for lithium ions.[175] Additionally, amorphous GeO_x nanoparticles less than 10 nm in size could mitigate the mechanical stress of volume change. Thus the obtained composites showed unique cyclic stability (1008 mAh g^{-1} for 100 cycles with retention of 96%) and rate performance (545 mAh g^{-1} even at 15 C) (**Figure 14**).[175]

Introduction of holes into the planar sheet is also a good choice to improve the electrochemical performance of GNS sheets, since the holes can provide a high density of cross plane diffusion channels for Li^+ ions.[101, 106, 138, 160, 241, 244, 245] Previous works indicated holey graphene (HG) prepared by HNO_3[257]and KOH etching[258] exhibited significantly improved electrochemical performance as an anode material for LIBs, such as better cycle performance and higher rate capability in comparison with graphene sheets, activated graphene sheets, bare SnO_2 and SnO_2–GNSs composites.[182]

4 Beyond morphologies

4.1 Composition

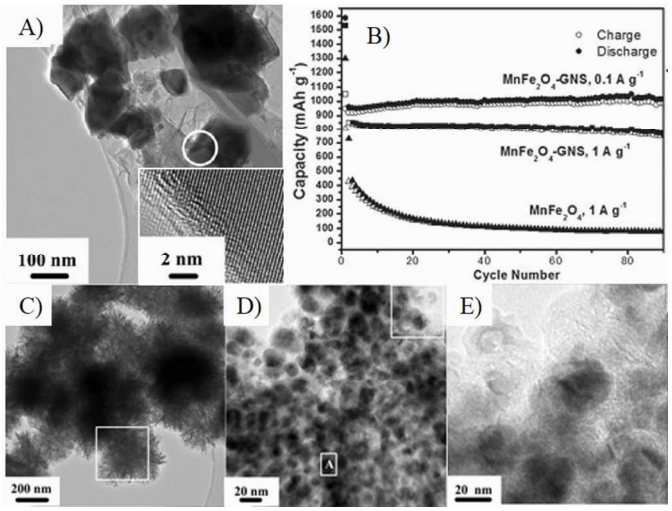

Figure 15. TEM image (A) and cyclic performances (B) of $MnFe_2O_4$–GNS composite. C–E, TEM image of $MnFe_2O_4$–GNSs nanocomposite after 70 charge–discharge process. [67] Reproduced from Ref. 67 with permission from The Royal Society of Chemistry.

RSC Advances Accepted Manuscript

The composition of MOs also plays a significantly role on the capacity, stability and rate performances of MOs–G nanocomposites. Firstly, most metal oxide anode materials are based on conversion reactions and alloy reactions. As a result, their theoretical capacities are tightly related with their compositions. For instance, Zn formed during conversion reactions can form alloys with Li, so $ZnFe_2O_4$ has a higher theoretical capacity of 1072 mAh g^{-1} than that of Fe_3O_4 (924 mAh g^{-1}).[259] But pure $ZnFe_2O_4$ has a reversible capacity of 957.7 mAh g^{-1}, while its graphene composites can reach to 1082 mAh g^{-1}.[204] Searching for other metal compounds with higher capacity is also a hot research topic. Metal carbonates, especially their graphene composites, can show higher capacities than their theoretical capacities.[260-262] For example, $CoCO_3$-graphene composites exhibited high capacities of over 1000 mAh g^{-1}, because both of the cations (Co^{2+}) and anions (CO_3^{2-}) are involved in the electron transfer.[263]

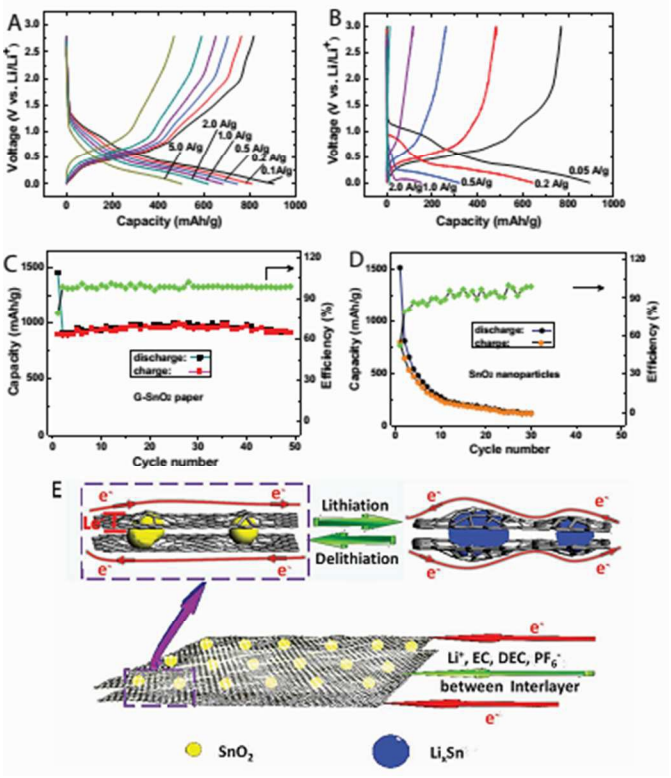

Figure 16. Charge/discharge curves of N–doped G–SnO_2 papers (A) and commercial SnO_2 nanoparticles (20–50 nm, B) at various current densities. Cycling performance of N–doped G–SnO_2 paper (C) and SnO_2 nanoparticles (D) at a current density of 50 mA g^{-1}. Schematic representation (E) showing paths for lithium–ions and electrons in the N–doped G–SnO_2 paper, respectively.[272] Reproduced with permission from Ref. 272 Copyright (2012) WILEY-VCH.

Recently, our researches on MFe_2O_4–GNS (M=Mn,[67] Co,[69] Ni[68]) nanocomposites indicated MFe_2O_4 could transform into the nanosized hybrid of Fe_3O_4 (MOs) with the size about 20 nm after discharge–charge process (**Figure 15**), and the *in–situ* formed hybrid of Fe_3O_4 (MOs) combined with GNSs to form a spongy porous structure, which could further accommodate its volume change and result in good stability of electrode. Additionally, the formed hybrid could also act as the matrix of MOs (Fe_3O_4) to prevent the aggregation and growth of the *in–situ* formed Fe_3O_4 (MOs) nanoparticles, and further lead to good cyclic stability. [67] Various graphene composites with multiple MOs, including $NiFe_2O_4$–graphene heteroarchitectures,[264] $CoFe_2O_4$/graphene sandwiched structures,[265] $ZnSnO_3$/graphene,[266] hollow Zn_2SnO_4 boxes@graphene and the incorporation of In_2O_3 into SnO_2,[192, 193] indicated that multiple MOs would improve the electrochemical activity and reduce the charge transfer resistance of electrodes, leading to the enhanced reversible capacity and rate capability. On the other hand, transferring the surface MOs to the corresponding high electron conductivity compounds, such as TiN,[235] SnS_2[56, 57, 267] or MoC,[268] would also improve the rate capability of composites. Furthermore, the doping of N,[97, 121, 269] F[270] and Boron[271] could significantly increase the conductivity of graphene, and further lead to the enhanced reversible capacity and rate capability. For example, the N–doped graphene–SnO_2 sandwiched films had a capacity of 504 mAh g^{-1} at 5 A g^{-1}, while the undoped graphene/SnO_2 films only reached to 526 mAh g^{-1} at 0.1 A g^{-1} (**Figure 16**).[158, 272]

4.2 Interaction

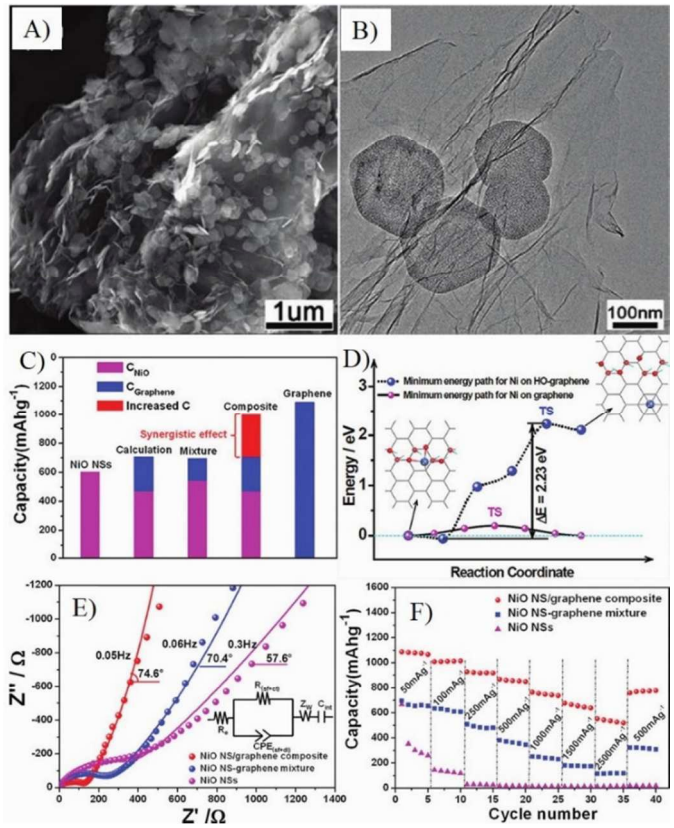

Figure 17. SEM (A) and TEM (B) images, capacity (C), interactions between graphene with oxygen functional groups and NiO (D), EIS spectra (E) and rate capability (E) of oxygen bridged NiO-Graphene composites.[274] Reproduced with permission from Ref. 274 Copyright (2012) American Chemical Society.

Based on above discussions, it can be found that the interactions between MOs nanomaterials and graphene greatly

RSC Advances Accepted Manuscript

This journal is © The Royal Society of Chemistry

affect the stability and charge transfer resistance of anodes, which are tightly related to the electrochemical lithium storage performances (cyclic stability and rate capability). For example, hollow porous Fe_3O_4 beads–rGO composites showed higher electrochemical performances than that of the mechanically mixed composites due to the *in–situ* formed strong interactions between Fe_3O_4 beads and rGO.[249] Graphene composites fabricated by co–assembly via electrostatic interactions also result in strong interactions between MOs nanomaterials and graphene, which can lead to composites in encapsulated and layered models with high mechanical and electrochemical stability and further reduce the charge transfer resistances.[72, 74-80, 245]

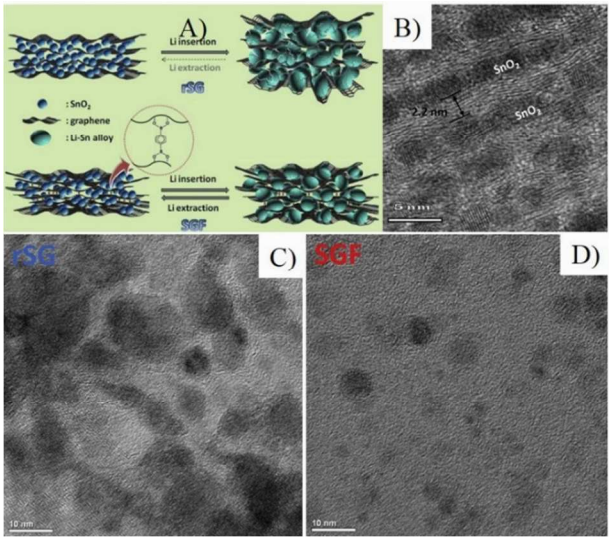

Figure 18. A, Schematic diagram depicting the different behaviors between rSG and SGF during Li alloying/dealloying. B, Ultramicrotomed cross–sectional view of SGF. HRTEM images of rSG (C) and SGF(D) after 50 cycles.[111] Reproduced from Ref. 111, Copyright (2013) with permission from Elsevier.

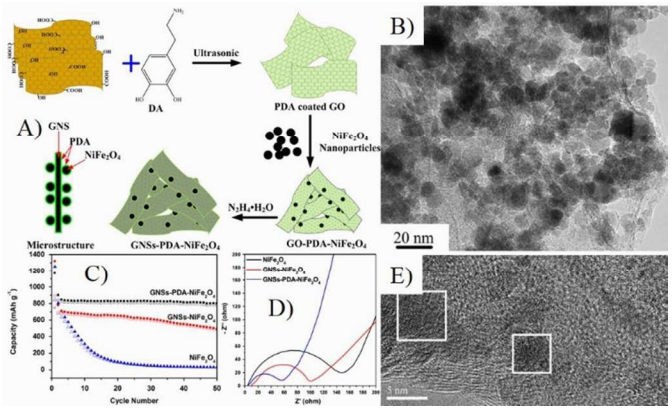

Figure 19. Schematic illustration of the possible formation mechanism (A), TEM image (B) and cyclic performances at 1 A g^{-1} (C), Nyquist plots (D) and TEM iamges after 50 cycles of GNSs–PDA–$NiFe_2O_4$ nanocomposites.[68] Reproduced from Ref. 68 Copyright (2014) with permission from Elsevier.

Covalently bonds can be generated between MOs nanomaterials and graphene by *in–situ* processes, in which the formation of nanomaterials and reduction of GO are occurred simultaneously.[184, 191, 273, 274] Detailed researches and density functional theory (DFT) calculations clearly indicated these bonds usually with O or N atoms on the surface of graphene acting as bridges, such as C–O–Ni,[274] C–O–Fe,[273] Sn–N–C and Sn–O–C[191] bonds. With the C–O–Ni bond as example (**Figure 17**), composites with this bond showed lower surface charge–transfer resistance (105.6 Ω) than the composite without bonding (213.3 Ω) or pure NiO nanosheets (279.9 Ω).[274]

Furthermore, the rich functional groups on graphene can react with cross–linking agent, such as benzene–1,4–diboronic acid (BDBA), to generate a graphene framework. The graphene framework can increase overall electron conductivity, confine/fix nanoparticles and avoid their aggregations during charge–discharge process (**Figure 18**).[111] Polymer coating on the composites can also increase structure stability, electrochemical activity and the interactions between oxides and graphene, and the graphene composites with conductive polymers, such as polyaniline[275, 276] and PEDOT,[277] have been invested and shown remarkable rate performances. Even the un–conductive polymers, such as polydopamine, can also reduce the charge transfer resistances and further lead to stable high rate performances (**Figure 19**).[68] These polymer coated graphene composites can also be transformed to carbon coated graphene composites by carbonization process, and the formed carbon shells tackle the deformation of MOs nanoparticles, keep the overall electrode highly conductive and active in lithium storage.[278]

Gel mixtures of GO, metal precursors and carbon precursors have been widely used to prepare graphene composites. After being electrospinned and carbonized, the obtained carbon coated graphene composites have unique lithium storage properties.[135, 213, 279, 280] Moreover, Ren et al. proved that the simultaneously formed carbon coating by the carbonization of glucose on the surface of the intermediate products (G–CrOOH) would provide more protections compared with the carbon layer post–formed by the carbonization of glucose on the surface of graphene–Cr_2O_3 composites. The simultaneously formed carbon layers could prevent the aggregations of Cr_2O_3 nanoparticles and limit their growth, whereas the latter could not effectively prevent the aggregation of nanoparticles because of mere coverage. As a result, the former carbon coated composites showed the improved electrochemical properties compared to the latter composites, such as higher reversible capacity, better cycle performance and rate capability.[131]

5. Conclusions

We have reviewed the applications of 3D MOs–G composites in LIBs, especially on the effects of morphology and size of MOs or graphene on the properties of graphene composites. The core idea to improve the electrochemical performances of graphene composites in LIBs is how to enhance the electron conductivity and the lithium diffusion. Thus MOs must have at least one dimension in nanoscale to reduce the lithium diffusion distance. While these nanomaterials also need to have enough contact sites and interactions with graphene, which will decide

RSC Advances Accepted Manuscript

the charge transfer resistance, mechanical and electrochemical stability. Furthermore, proper pore size distribution is important for electrolyte accessing. To meet all above, one of the MOs or graphene must be in 3D structures. On the other hand, the composition of graphene composites and the interactions between graphene and MOs also affect their electrochemical performances.

Although considerable researches and breakthroughs have been achieved, challenges of using graphene composites for lithium storage still remain. The fundamental question is the cost–effective, environmentally friend and sustainable approach to large–scale production of high quality graphene or GO. Right now, beginning from graphite is still the most ideal route due to the abundant reserves of graphite. In past years, it is believed that the physical exfoliation method is not suitable for mass production even though it can produce high quality graphene. However, good news come from European[281] and China[282] recently. Defect free graphene with few layers can be prepared in large–scale by high–shear mixing of graphite in suitable stabilizing liquids or using a supercritical CO_2 combined with ultrasound approach.[281, 282] Secondly, graphene composites anodes always show low initial efficiency and few of them can reach to 75%,[163, 167, 228, 273] which will cause many issues in full battery. The low initial efficiency mainly derives from the formation of SEI film on the surface of graphene composites with large surface area and the side reactions of functional groups on graphene, so high quality graphene is required and the surface area of the composites should be optimized. Thirdly, the capacity of transition MOs–G composites usually increases with the increasing cycles, and always much higher than their initial and theoretical capacity, which is considered as the decomposition of electrolyte catalyzed by MOs.[68, 81, 204, 243] This is also an very important problem for safety issues. In aim of final industrial implementation, large scale, low cost and simple production of graphene composites with high electrochemical lithium storage performances is one of the most important challenges. The road of realizing 3D MOs–graphene composites in LIBs is tortuous. But, with continues exploitations the future is bright!

Acknowledgements

The work was supported by the National Basic Research Program of China (2014CB239700), Shanghai Nano–Project (12nm0503502) Program of National Natural Science Foundation of China (21371121 and 21331004) and Minhang District Developing Project, Science and Technology Commission of Shanghai Municipality (14DZ2250800).

Notes and references

Shanghai Electrochemical Energy Devices Research Center, School of Chemistry and Chemical Engineering and State Key Laboratory of Metal Matrix Composites, Shanghai Jiao Tong University,, Shanghai, 200240 (P. R. China). Fax: +86-21-54741297; Tel: +86-21-54743262; E-mail: xfqian@sjtu.edu.cn

1. L. Zhang, *China's urban development report No.7*, http://www.china.com.cn/opinion/think/2014-09/17/content_33532822.htm, Accessed Sept 17th, 2014.
2. J. W. Kim, J. D. Ocon, D.-W. Park, *et al.*, *ChemSusChem*, 2014, **7**, 1265.
3. V. Chabot, D. Higgins, A. Yu, *et al.*, *Energ Environ Sci*, 2014, **7**, 1564.
4. C. Xu, B. Xu, Y. Gu, *et al.*, *Energ Environ Sci*, 2013, **6**, 1388.
5. D. Wei and J. Kivioja, *Nanoscale*, 2013, **5**, 10108.
6. L. W. Su, Y. Jing and Z. Zhou, *Nanoscale*, 2011, **3**, 3967.
7. B. Li, J. Zai, Y. Xiao, *et al.*, *CrystEngComm*, 2014, **16**, 3318.
8. R. Yi, J. Zai, F. Dai, *et al.*, *Electrochem Commun*, 2013, **36**, 29.
9. J. C. Shelton, H. R. Patil and J. M. Blakely, *Surf Sci*, 1974, **43**, 493.
10. C. Oshima and A. Nagashima, *J Phys-condens Mat*, 1997, **9**, 1.
11. X. K. Lu, M. F. Yu, H. Huang, *et al.*, *Nanotechnology*, 1999, **10**, 269.
12. K. S. Novoselov, A. K. Geim, S. V. Morozov, *et al.*, *Science*, 2004, **306**, 666.
13. J. Zhu, M. Chen, Q. He, *et al.*, *Rsc Adv*, 2013, **3**, 22790.
14. Q. Xiang, J. Yu and M. Jaroniec, *Chem Soc Rev*, 2012, **41**, 782.
15. R. S. Edwards and K. S. Coleman, *Accounts Chem Res*, 2013, **46**, 23.
16. D. Chen, H. Feng and J. Li, *Chem Rev*, 2012, **112**, 6027.
17. Y. Sun and G. Shi, *J Polym Sci Pol Phys*, 2013, **51**, 231.
18. A. Alarcon, N. Viet-Hung, S. Berrada, *et al.*, *IEEE T Electron Dev*, 2013, **60**, 985.
19. J. Cayssol, B. Huard and D. Goldhaber-Gordon, *Phys Rev B*, 2009, **79**.
20. J. Liu, M. Durstock and L. Dai, *Energ Environ Sci*, 2014, **7**, 1297.
21. P. Avouris, *Proceedings 2010 10th IEEE International Conference on Nanotechnology and Joint Symposium with Nano Korea 2010 KINTEX (IEEE-NANO 2010)*, 2010, 6.
22. D. Gunlycke, D. A. Areshkin, J. Li, *et al.*, *Nano Lett*, 2007, **7**, 3608.
23. D. Yong-Joo and Y. Gyu-Chul, *Nanotechnology*, 2010, **21**, 105204.
24. R. Arsat, M. Breedon, M. Shafiei, *et al.*, *Chem Phys Lett*, 2009, **467**, 344.
25. H. Song, L. Zhang, C. He, *et al.*, *J Mater Chem*, 2011, **21**, 5972.
26. T. Kuila, S. Bose, P. Khanra, *et al.*, *Biosens Bioelectron*, 2011, **26**, 4637.
27. D. Zhao, Z. Li, L. Liu, *et al.*, *Acta Chim Sinica*, 2014, **72**, 185.
28. H. Jiang, *Small*, 2011, **7**, 2413.
29. P. V. Kamat, *J Phys Chem Lett*, 2011, **2**, 242.
30. S.-S. Yu and W.-T. Zheng, *Nanoscale*, 2010, **2**, 1069.
31. C. Huang, C. Li and G. Shi, *Energ Environ Sci*, 2012, **5**, 8848.
32. L.-L. Tan, S.-P. Chai and A. R. Mohamed, *Chemsuschem*, 2012, **5**, 1868.
33. H. Tian, S. Ma, H.-M. Zhao, *et al.*, *Nanoscale*, 2013, **5**, 8951.
34. G. K. Dimitrakakis, E. Tylianakis and G. E. Froudakis, *Nano Lett*, 2008, **8**, 3166.
35. S. Yang, L. Zhan, X. Xu, *et al.*, *Adv Mater*, 2013, **25**, 2130.
36. L. Dai, *Accounts Chem Res*, 2013, **46**, 31.
37. S. Guo and S. Dong, *Chem Soc Rev*, 2011, **40**, 2644.

RSC Advances Accepted Manuscript

 This journal is © The Royal Society of Chemistry

38. H. Gwon, H.-S. Kim, K. U. Lee, *et al.*, *Energ Environ Sci*, 2011, **4**, 1277.
39. H. Junbo, S. Yuyan, M. W. Ellis, *et al.*, *Phys Chem Chem Phys*, 2011, **13**, 15384.
40. T. Kuila, A. K. Mishra, P. Khanra, *et al.*, *Nanoscale*, 2013, **5**, 52.
41. I. V. Lightcap and P. V. Kamat, *Accounts Chem Res*, 2013, **46**, 2235.
42. B. Luo, S. Liu and L. Zhi, *Small*, 2012, **8**, 630.
43. M. Pumera, *Energ Environ Sci*, 2011, **4**, 668.
44. D. Zhou, Y. Cui and B. Han, *Chinese Sci Bull*, 2012, **57**, 2983.
45. J. Liu, Y. Xue, M. Zhang, *et al.*, *Mrs Bull*, 2012, **37**, 1265.
46. Y. Sun, Q. Wu and G. Shi, *Energ Environ Sci*, 2011, **4**, 1113.
47. L. Grande, V. T. Chundi, D. Wei, *et al.*, *Particuology*, 2012, **10**, 1.
48. X. Wan, Y. Huang and Y. Chen, *Accounts Chem Res*, 2012, **45**, 598.
49. Z.-S. Wu, G. Zhou, L.-C. Yin, *et al.*, *Nano Energy*, 2012, **1**, 107.
50. M. Xu, Y. Gao, X. Yang, *et al.*, *Chinese Sci Bull*, 2012, **57**, 3000.
51. G. Zhao, T. Wen, C. Chen, *et al.*, *Rsc Adv*, 2012, **2**, 9286.
52. Q. Tang, Z. Zhou and Z. F. Chen, *Nanoscale*, 2013, **5**, 4541.
53. V. Z. Mordkovich, *Synthetic Met*, 1996, **80**, 243.
54. G. Wang, X. Shen, J. Yao, *et al.*, *Carbon*, 2009, **47**, 2049.
55. P. G. Bruce, B. Scrosati and J. M. Tarascon, *Angew Chem Int Edit*, 2008, **47**, 2930.
56. J. Zai, K. Wang, Y. Su, *et al.*, *J Power Sources*, 2011, **196**, 3650.
57. J. Zai, X. Qian, K. Wang, *et al.*, *CrystEngComm*, 2012, **14**, 1364.
58. Y. Li, Z.-Y. Fu and B.-L. Su, *Adv Funct Mater*, 2012, **22**, 4634.
59. C. N. R. Rao, H. S. S. R. Matte and K. S. Subrahmanyam, *Accounts Chem Res*, 2013, **46**, 149.
60. S. Han, D. Wu, S. Li, *et al.*, *Small*, 2013, **9**, 1173.
61. V. Georgakilas, M. Otyepka, A. B. Bourlinos, *et al.*, *Chem Rev*, 2012, **112**, 6156.
62. Y. Zhu, D. K. James and J. M. Tour, *Adv Mater*, 2012, **24**, 4924.
63. W. I. Park, C.-H. Lee, J. M. Lee, *et al.*, *Nanoscale*, 2011, **3**, 3522.
64. X. Huang, X. Qi, F. Boey, *et al.*, *Chem Soc Rev*, 2012, **41**, 666.
65. S.-M. Paek, E. Yoo and I. Honma, *Nano Lett*, 2009, **9**, 72.
66. L. Tao, J. Zai, K. Wang, *et al.*, *Rsc Adv*, 2012, **2**, 3410.
67. Y. Xiao, J. Zai, L. Tao, *et al.*, *Phys Chem Chem Phys*, 2013, **15**, 3939.
68. Y. Xiao, J. Zai, X. Li, *et al.*, *Nano Energy*, 2014, **6**, 51.
69. Y. Xiao, X. Li, J. Zai, *et al.*, *Nano-Micro Lett*, 2014.
70. A. K. Rai, L. T. Anh, J. Gim, *et al.*, *J Power Sources*, 2013, **244**, 435.
71. Z. Chen, M. Zhou, Y. Cao, *et al.*, *Adv Energy Mater*, 2012, **2**, 95.
72. X.-l. Huang, J. Chai, T. Jiang, *et al.*, *J Mater Chem*, 2012, **22**, 3404.
73. H. Xiao-lei, W. Ru-zhi, X. Dan, *et al.*, *Adv Funct Mater*, 2013, **23**, 4345.
74. S. Yang, X. Feng, S. Ivanovici, *et al.*, *Angew Chem Int Edit*, 2010, **49**, 8408.
75. W. Wei, S. Yang, H. Zhou, *et al.*, *Adv Mater*, 2013, **25**, 2909.
76. T. Yoon, J. Kim, J. Kim, *et al.*, *Energies*, 2013, **6**, 4830.
77. Y. Luo, J. Luo, W. Zhou, *et al.*, *J Mater Chem A*, 2013, **1**, 273.
78. R. Yi, J. Zai, F. Dai, *et al.*, *Nano Energy*, 2014, **6**, 211.
79. X. Yang, K. Fan, Y. Zhu, *et al.*, *Acs Appl Mater Inter*, 2013, **5**, 997.
80. S. J. R. Prabakar, Y.-H. Hwang, E.-G. Bae, *et al.*, *Adv Mater*, 2013, **25**, 3307.
81. Z.-S. Wu, W. Ren, L. Wen, *et al.*, *Acs Nano*, 2010, **4**, 3187.
82. L. Tao, J. Zai, K. Wang, *et al.*, *J Power Sources*, 2012, **202**, 230.
83. Y.-J. Hu, J. Jin, H. Zhang, *et al.*, *Acta Phys-chim Sin*, 2010, **26**, 2073.
84. P. Lue, Y. Feng, X. Zhang, *et al.*, *Sci China Technol Sci*, 2010, **53**, 2311.
85. J. N. Coleman, *Accounts Chem Res*, 2013, **46**, 14.
86. D. Wang, D. Choi, J. Li, *et al.*, *Acs Nano*, 2009, **3**, 907.
87. D. Wang, R. Kou, D. Choi, *et al.*, *Acs Nano*, 2010, **4**, 1587.
88. L. Pan, H. Zhao, W. Shen, *et al.*, *J Mater Chem A*, 2013, **1**, 7159.
89. Y. Chen, B. Song, L. Lu, *et al.*, *Nanoscale*, 2013, **5**, 6797.
90. Q. Han, J. Zai, Y. Xiao, *et al.*, *Rsc Adv*, 2013, **3**, 20573.
91. Y. Sheng, Y. Wenbo, Z. Jia, *et al.*, *Adv Funct Mater*, 2013, **23**, 91.
92. S. X. Yu, L. W. Yang, Y. Tian, *et al.*, *J Mater Chem A*, 2013, **1**, 12750.
93. Z. Zhang, Y. Wang, D. Li, *et al.*, *Ind Eng Chem Res*, 2013, **52**, 14906.
94. H. Sun, X. Sun, T. Hu, *et al.*, *J Phys Chem C*, 2014, **118**, 2263.
95. J. Zhang, S. Wan, B. Yan, *et al.*, *J Nanosci Nanotechno*, 2013, **13**, 4364.
96. S. Bai, S. Chen, X. Shen, *et al.*, *Rsc Adv*, 2012, **2**, 10977.
97. F. Zou, X. Hu, Y. Sun, *et al.*, *Chem-eur J*, 2013, **19**, 6027.
98. X. Chaohe, S. Jing and G. Lian, *Nanoscale*, 2012, **4**, 5425.
99. X. Chaohe, S. Jing and G. Lian, *J Mater Chem*, 2012, **22**, 975.
100. M. Yu, H. Sun, X. Sun, *et al.*, *Mater Lett*, 2013, **108**, 29.
101. Y. Zhang, H. Liu, Z. Zhu, *et al.*, *Electrochim Acta*, 2013, **108**, 465.
102. J. Wang, Y. Zhou, B. Xiong, *et al.*, *Electrochim Acta*, 2013, **88**, 847.
103. Y. Chen, M. Zhuo, J. Deng, *et al.*, *J Mater Chem A*, 2014, **2**, 4449.
104. H. Huang, J. Fang, Y. Xia, *et al.*, *J Mater Chem A*, 2013, **1**, 2495.
105. Y. Dong, S. Li, H. Xu, *et al.*, *Phys Chem Chem Phys*, 2013, **15**, 17165.
106. S. Yongming, H. Xianluo, L. Wei, *et al.*, *Adv Funct Mater*, 2013, **23**, 2436.
107. Z. Zhang, Q. Chu, H. Li, *et al.*, *J Colloid Interf Sci*, 2013, **409**, 38.
108. S. Yaodong, C. Jun Song, Z. Jixin, *et al.*, *J Nanopart Res*, 2013, **15**, 1913 (8 pp.).
109. W. Bao, W. Xing-Long, S. Chun-Ying, *et al.*, *J Mater Chem*, 2010, **20**, 10661.
110. L. Q. Lu and Y. Wang, *Electrochem Commun*, 2012, **14**, 82.
111. H. Yun-Hwa, B. Eun Gyoung, S. Kee-Sun, *et al.*, *J Power Sources*, 2013, **240**, 683.
112. G. Qi, Z. Zhe, G. Hailing, *et al.*, *J Power Sources*, 2013, **240**, 149.
113. B. Zhao, G. Zhang, J. Song, *et al.*, *Electrochim Acta*, 2011, **56**, 7340.
114. J. Zhu, T. Zhu, X. Zhou, *et al.*, *Nanoscale*, 2011, **3**, 1084.
115. Z. Ming, Q. Baihua, D. Lei, *et al.*, *J Mater Chem*, 2012, **22**, 3868.
116. S.-K. Park, S.-H. Yu, N. Pinna, *et al.*, *J Mater Chem*, 2012, **22**, 2520.
117. S. Yang, Y. Gong, Z. Liu, *et al.*, *Nano Lett*, 2013, **13**, 1596.
118. J. Shuhua, Y. Wenbo, G. Ziqi, *et al.*, *J Mater Sci*, 2013, **48**, 3870.
119. J. Qu, Y. Yan, Y.-X. Yin, *et al.*, *Acs Appl Mater Inter*, 2013, **5**, 5777.
120. D. W.-P. Pang, F.-W. Yuan, Y.-C. Chang, *et al.*, *Nanoscale*, 2012, **4**, 4562.

RSC Advances Accepted Manuscript

121. S.-K. Park, A. Jin, S.-H. Yu, *et al.*, *Electrochim Acta*, 2014, **120**, 452.
122. X. Chi, L. Chang, D. Xie, *et al.*, *Mater Lett*, 2013, **106**, 178.
123. L. Noerochim, J.-Z. Wang, D. Wexler, *et al.*, *J Power Sources*, 2013, **228**, 198.
124. F. Xiao-Yong, S. Xiao-Yuan, W. Jing, *et al.*, *J Solid State Electr*, 2013, **17**, 201.
125. C. Nethravathi, B. Viswanath, J. Michael, *et al.*, *Carbon*, 2012, **50**, 4839.
126. L. Tian, Q. Zhuang, J. Li, *et al.*, *Electrochim Acta*, 2012, **65**, 153.
127. J. Qu, Y.-X. Yin, Y.-Q. Wang, *et al.*, *Acs Appl Mater Inter*, 2013, **5**, 3932.
128. P. Lian, J. Wang, D. Cai, *et al.*, *Electrochim Acta*, 2014, **116**, 103.
129. Y. Zhu, C. Li and C. Cao, *Rsc Adv*, 2013, **3**, 11860.
130. M. Zhang, M. Jia, Y. Jin, *et al.*, *J Alloy Compd*, 2013, **566**, 131.
131. W. Yue, S. Tao, J. Fu, *et al.*, *Carbon*, 2013, **65**, 97.
132. D. Qiu, L. Ma, M. Zheng, *et al.*, *Mater Lett*, 2012, **84**, 9.
133. D. Yucheng, M. Ruguang, H. Mingjun, *et al.*, *Phys Chem Chem Phys*, 2013, **15**, 7174.
134. Y. Jiang, T. Yuan, W. Sun, *et al.*, *Acs Appl Mater Inter*, 2012, **4**, 6216.
135. J. Zhu, G. Zhang, X. Yu, *et al.*, *Nano Energy*, 2014, **3**, 80.
136. Z. Jian, L. Danni, Z. Guanhua, *et al.*, *Nanoscale*, 2013, **5**, 5499.
137. M. Zhang, D. Lei, X. Yin, *et al.*, *J Mater Chem*, 2010, **20**, 5538.
138. S. Q. Chen and Y. Wang, *J Mater Chem*, 2010, **20**, 9735.
139. X. Zhu, Y. Zhu, S. Murali, *et al.*, *Acs Nano*, 2011, **5**, 3333.
140. S.-H. Yu, D. E. Conte, S. Baek, *et al.*, *Adv Funct Mater*, 2013, **23**, 4293.
141. C. Zhong, J. Wang, Z. Chen, *et al.*, *J Phys Chem C*, 2011, **115**, 25115.
142. T. Chen, L. Pan, X. Liu, *et al.*, *Rsc Adv*, 2012, **2**, 11719.
143. L. Li, Z. Guo, A. Du, *et al.*, *J Mater Chem*, 2012, **22**, 3600.
144. N. Li, Y. Xiao, C. Hu, *et al.*, *Chem-Asian J*, 2013, **8**, 1960.
145. J. W. Ko, S.-W. Kim, J. Hong, *et al.*, *Green Chem*, 2012, **14**, 2391.
146. J. Qiu, P. Zhang, M. Ling, *et al.*, *Acs Appl Mater Inter*, 2012, **4**, 3636.
147. K. Gil-Pyo, N. Inho, K. Nam Dong, *et al.*, *Electrochem Commun*, 2012, **22**, 93.
148. X. Meng, D. Geng, J. Liu, *et al.*, *Nanotechnology*, 2011, **22**, 165602.
149. E. B. Nursanto, A. Nugroho, S.-A. Hong, *et al.*, *Green Chem*, 2011, **13**, 2714.
150. L. Zhuo, Y. Wu, W. Zhou, *et al.*, *Acs Appl Mater Inter*, 2013, **5**, 7065.
151. L. Zhuo, Y. Wu, L. Wang, *et al.*, *J Mater Chem A*, 2013, **1**, 3954.
152. A. K. Rai, J. Gim, A. Ly Tuan, *et al.*, *Electrochim Acta*, 2013, **100**, 63.
153. D. Li, D. Shi, Z. Chen, *et al.*, *Rsc Adv*, 2013, **3**, 5003.
154. J. Xiao, G. Xu, S.-G. Sun, *et al.*, *Part Part Syst Char*, 2013, **30**, 893.
155. Y. Qi, H. Zhang, N. Du, *et al.*, *J Mater Chem A*, 2013, **1**, 2337.
156. H. Xin, C. Jing, Y. Hong, *et al.*, *J Mater Chem A*, 2013, **1**, 6901.
157. Y. Sun, X. Hu, W. Luo, *et al.*, *J Mater Chem A*, 2013, **1**, 4468.
158. G. Xia, N. Li, D. Li, *et al.*, *Acs Appl Mater Inter*, 2013, **5**, 8607.
159. G. Wang, H. Wang, S. Cai, *et al.*, *J Power Sources*, 2013, **239**, 37.
160. L. Li, G. Zhou, Z. Weng, *et al.*, *Carbon*, 2014, **67**, 500.
161. G.-W. Zhou, J. Wang, P. Gao, *et al.*, *Ind Eng Chem Res*, 2013, **52**, 1197.
162. C. Zhao, S.-L. Chou, Y. Wang, *et al.*, *Rsc Adv*, 2013, **3**, 16597.
163. W. Xiao, Z. Wang, H. Guo, *et al.*, *Appl Surf Sci*, 2013, **266**, 148.
164. L. Xiao, D. Wu, S. Han, *et al.*, *Acs Appl Mater Inter*, 2013, **5**, 3764.
165. D. Meng, X. Chaohe, S. Jing, *et al.*, *J Mater Chem A*, 2013, **1**, 7154.
166. B. Jang, O. B. Chae, S.-K. Park, *et al.*, *J Mater Chem A*, 2013, **1**, 15442.
167. D. Chen, H. Quan, J. Liang, *et al.*, *Nanoscale*, 2013, **5**, 9684.
168. X. Huang, B. Sun, S. Chen, *et al.*, *Chem-Asian J*, 2014, **9**, 206.
169. M. Cai, H. Qian, Z. Wei, *et al.*, *Rsc Adv*, 2014, **4**, 6379.
170. M. Zhang and M. Jia, *J Alloy Compd*, 2013, **551**, 53.
171. A. Hu, X. Chen, Y. Tang, *et al.*, *Mater Lett*, 2013, **91**, 315.
172. Y. Chang, J. Li, B. Wang, *et al.*, *J Mater Chem A*, 2013, **1**, 14658.
173. Y. Sun, X. Hu, W. Luo, *et al.*, *Acs Appl Mater Inter*, 2013, **5**, 10145.
174. W. Yue, S. Jiang, W. Huang, *et al.*, *J Mater Chem A*, 2013, **1**, 6928.
175. S. Jin, N. Li, H. Cui, *et al.*, *Nano Energy*, 2013, **2**, 1128.
176. S. Wu, Y. Zhu, C. Li, *et al.*, *J Alloy Compd*, 2014, **582**, 289.
177. Z. Xiaoyi, L. Jianjiang, S. Xilin, *et al.*, *Adv Mater Res*, 2013, **709**, 157.
178. Y. Chen, X. Di, C. Ma, *et al.*, *Rsc Adv*, 2013, **3**, 17659.
179. D. Zhou, H. Wu, Z. Wei, *et al.*, *Phys Chem Chem Phys*, 2013, **15**, 16898.
180. G.-P. Kim, I. Nam, S. Park, *et al.*, *Nanotechnology*, 2013, **24**.
181. C. Jianli, X. Huolin, Z. Haimei, *et al.*, *J Power Sources*, 2013, **232**, 152.
182. Y. Yang, X. Ji, F. Lu, *et al.*, *Phys Chem Chem Phys*, 2013, **15**, 15098.
183. B. P. Vinayan and S. Ramaprabhu, *J Mater Chem A*, 2013, **1**, 3865.
184. H. Song, N. Li, H. Cui, *et al.*, *J Mater Chem A*, 2013, **1**, 7558.
185. J. Lin, Z. Peng, C. Xiang, *et al.*, *Acs Nano*, 2013, **7**, 6001.
186. J. Liang, Y. Liu, L. Guo, *et al.*, *Rsc Adv*, 2013, **3**, 11489.
187. Z. Junsheng, W. Dianlong and W. Lin, *Ionics*, 2013, **19**, 1223.
188. Y. Huang, D. Wu, S. Han, *et al.*, *Chemsuschem*, 2013, **6**, 1510.
189. Q. Guo and X. Qin, *Ecs Solid State Letters*, 2013, **2**, M41.
190. C. Gu, H. Zhang, X. Wang, *et al.*, *Mater Res Bull*, 2013, **48**, 4112.
191. X. Zhou, L.-J. Wan and Y.-G. Guo, *Adv Mater*, 2013, **25**, 2152.
192. H. Yang, T. Song, S. Lee, *et al.*, *Electrochim Acta*, 2013, **91**, 275.
193. W. Xing, X. Wang, L. Song, *et al.*, *Mater Chem Phys*, 2013, **140**, 441.
194. R. Huang, H. Ge, X. Lin, *et al.*, *Rsc Adv*, 2013, **3**, 1235.
195. M. Zhen, L. Su, Z. Yuan, *et al.*, *Rsc Adv*, 2013, **3**, 13696.
196. H. Tao, S. Xiang, S. Hongtao, *et al.*, *Carbon*, 2013, **51**, 322.
197. D. Li, D. Shi, Z. Liu, *et al.*, *J Nanopart Res*, 2013, **15**.
198. C. Dandan, L. Dongdong, W. Suqing, *et al.*, *J Alloy Compd*, 2013, **561**, 54.
199. C. Ban, M. Xie, X. Sun, *et al.*, *Nanotechnology*, 2013, **24**.
200. X. Jiang, X. Yang, Y. Zhu, *et al.*, *New J Chem*, 2013, **37**, 3671.
201. C. Han, M. Yan, L. Mai, *et al.*, *Nano Energy*, 2013, **2**, 916.
202. H. Zhao, L. Pan, S. Xing, *et al.*, *J Power Sources*, 2013, **222**, 21.
203. W. Song, J. Xie, W. Hu, *et al.*, *J Power Sources*, 2013, **229**, 6.
204. H. Xia, Y. Qian, Y. Fu, *et al.*, *Solid State Sci*, 2013, **17**, 67.

RSC Advances Accepted Manuscript

 This journal is © The Royal Society of Chemistry

205. X. Sun, C. Zhou, M. Xie, *et al.*, *J Mater Chem A*, 2014, **2**, 7319.
206. L. Zhang, Z. Wang, L. Wang, *et al.*, *Mater Lett*, 2013, **108**, 9.
207. Z. Chen, Y. Yan, S. Xin, *et al.*, *J Mater Chem A*, 2013, **1**, 11404.
208. R. Wang, C. Xu, J. Sun, *et al.*, *J Mater Chem A*, 2013, **1**, 1794.
209. A. Hu, X. Chen, Y. Tang, *et al.*, *Electrochem Commun*, 2013, **28**, 139.
210. Y. Chen, C. Yan and O. G. Schmidt, *Adv Energy Mater*, 2013, **3**, 1269.
211. F. Tu, T. Wu, S. Liu, *et al.*, *Electrochim Acta*, 2013, **106**, 406.
212. J. G. Radich, Y.-S. Chen and P. V. Kamat, *Ecs J Solid State Sci Technol*, 2013, **2**, M3178.
213. J. Zhu, D. Lei, G. Zhang, *et al.*, *Nanoscale*, 2013, **5**, 5499.
214. D. Wang, J. Yang, X. Li, *et al.*, *Energ Environ Sci*, 2013, **6**, 2900.
215. H. Juan, W. Rong, Z. Pengjun, *et al.*, *Mater Lett*, 2013, **100**, 173.
216. H. Juan, W. Rong, Z. Pengjun, *et al.*, *Integr Ferroelectr*, 2013, **144**, 66.
217. F. Zou, X. Hu, L. Qie, *et al.*, *Nanoscale*, 2014, **6**, 924.
218. Y. Li, Y. Wang and Y. Zhang, *Sci Adv Mater*, 2013, **5**, 523.
219. Y. Liu, W. Wang, L. Gu, *et al.*, *Acs Appl Mater Inter*, 2013, **5**, 9850.
220. S. Chen, P. Bao and G. Wan, *Nano Energy*, 2013, **2**, 425.
221. X. Wang, W. Tian, D. Liu, *et al.*, *Nano Energy*, 2013, **2**, 257.
222. H. Liu, J. Huang, C. Xiang, *et al.*, *J Mater Sci-mater El*, 2013, **24**, 3640.
223. N. Li, G. Zhou, R. Fang, *et al.*, *Nanoscale*, 2013, **5**, 7780.
224. Y. Tang, D. Wu, S. Chen, *et al.*, *Energ Environ Sci*, 2013, **6**, 2447.
225. J. Cheng, B. Wang, H. L. Xin, *et al.*, *J Mater Chem A*, 2013, **1**, 10814.
226. C. Nethravathi, C. R. Rajamathi, M. Rajamathi, *et al.*, *Acs Appl Mater Inter*, 2013, **5**, 2708.
227. X. Cao, B. Zheng, X. Rui, *et al.*, *Angew Chem Int Edit*, 2014, **53**, 1404.
228. Q. Zhou, Z. Zhao, Z. Wang, *et al.*, *Nanoscale*, 2014, **6**, 2286.
229. J. Zhu, D. Yang, X. Rui, *et al.*, *Small*, 2013, **9**, 3390.
230. S. Tao, W. Yue, M. Zhong, *et al.*, *Acs Appl Mater Inter*, 2014, **6**, 6332.
231. L. Zhao, W. Yue and Y. Ren, *Electrochim Acta*, 2014, **116**, 31.
232. G. Ji, B. Ding, Z. Sha, *et al.*, *Nanoscale*, 2013, **5**, 5965.
233. Y. Zhao, Y. Huang, W. Zhang, *et al.*, *Rsc Adv*, 2013, **3**, 23489.
234. C. Xu, X. Wang, L. Yang, *et al.*, *J Solid State Chem*, 2009, **182**, 2486.
235. Y. Qiu, K. Yan, S. Yang, *et al.*, *Acs Nano*, 2010, **4**, 6515.
236. Y. Xia, P. Yang, Y. Sun, *et al.*, *Adv Mater*, 2003, **15**, 353.
237. M. Kwiat, S. Cohen, A. Pevzner, *et al.*, *Nano Today*, 2013, **8**, 677.
238. Z. L. Wang, *Adv Mater*, 2000, **12**, 1295.
239. Y. Zou, J. Kan and Y. Wang, *J Phys Chem C*, 2011, **115**, 20747.
240. A. Yu, H. W. Park, A. Davies, *et al.*, *J Phys Chem Lett*, 2011, **2**, 1855.
241. Z. Yuqin and W. Yong, *Nanoscale*, 2011, **3**, 2615.
242. Y.-S. He, D.-W. Bai, X. Yang, *et al.*, *Electrochem Commun*, 2010, **12**, 570.
243. H. Xia, D. Zhu, Y. Fu, *et al.*, *Electrochim Acta*, 2012, **83**, 166.
244. J. Zai, C. Yu, L. Tao, *et al.*, *CrystEngComm*, 2013, **15**, 6663.
245. H. Yun, H. Xiao-lei, L. Jian-she, *et al.*, *J Mater Chem*, 2012, **22**, 2844.
246. K. Haegyeom, K. Sung-Wook, P. Young-Uk, *et al.*, *Nano Research*, 2010, **3**, 813.
247. X. Rui, J. Zhu, D. Sim, *et al.*, *Nanoscale*, 2011, **3**, 4752.
248. Q. Zou, J.-T. Zai, P. Liu, *et al.*, *Chem J Chinese U*, 2011, **32**, 630.
249. Y. Chen, B. Song, X. Tang, *et al.*, *J Mater Chem*, 2012, **22**, 17656.
250. C. Huagiang, L. Baojun, Z. Jingxian, *et al.*, *J Mater Chem*, 2012, **22**, 9759.
251. L. Na, L. Gang, Z. Chao, *et al.*, *Adv Funct Mater*, 2011, **21**, 1717.
252. Y. Wenbo, L. Zhenzhen, J. Shuhua, *et al.*, *J Mater Chem*, 2012, **22**, 16318.
253. X. Yang, K. Fan, Y. Zhu, *et al.*, *J Mater Chem*, 2012, **22**, 17278.
254. B. G. Choi, S.-J. Chang, Y. B. Lee, *et al.*, *Nanoscale*, 2012, **4**, 5924.
255. X. Zhu, G. Ning, X. Ma, *et al.*, *J Mater Chem A*, 2013, **1**, 14023.
256. J. Zai, C. Yu, Q. Zou, *et al.*, *Rsc Adv*, 2012, **2**, 4397.
257. X. Zhao, C. M. Hayner, M. C. Kung, *et al.*, *ACS Nano*, 2011, **5**, 8739.
258. J. Zhongging, P. Bo and A. Manthiram, *J Mater Chem A*, 2013, **1**, 7775.
259. Y. Ding, Y. F. Yang and H. X. Shao, *Electrochim Acta*, 2011, **56**, 9433.
260. S. Mirhashemihaghighi, B. Leon, C. P. Vicente, *et al.*, *Inorg Chem*, 2012, **51**, 5554.
261. M. J. Aragon, C. Perez-Vicente and J. L. Tirado, *Electrochem Commun*, 2007, **9**, 1744.
262. M. J. Aragon, B. Leon, C. P. Vicente, *et al.*, *J Power Sources*, 2011, **196**, 2863.
263. L. W. Su, Z. Zhou, X. Qin, *et al.*, *Nano Energy*, 2013, **2**, 276.
264. Y. Fu, Y. Wan, H. Xia, *et al.*, *J Power Sources*, 2012, **213**, 338.
265. S. Liu, J. Xie, C. Fang, *et al.*, *J Mater Chem*, 2012, **22**, 19738.
266. W. Song, J. Xie, S. Liu, *et al.*, *J Mater Res*, 2012, **27**, 3096.
267. J. Zhu, D. Wang, L. Wang, *et al.*, *Electrochim Acta*, 2013, **91**, 323.
268. H.-J. Zhang, K.-X. Wang, X.-Y. Wu, *et al.*, *Adv Funct Mater*, 2014, **24**, 3399.
269. A. L. M. Reddy, A. Srivastava, S. R. Gowda, *et al.*, *Acs Nano*, 2010, **4**, 6337.
270. H. Tachikawa, T. Iyama and H. Kawabata, *Jpn J Appl Phys*, 2010, **49**.
271. X. Wang, Z. Zeng, H. Ahn, *et al.*, *Appl Phys Lett*, 2009, **95**.
272. X. Wang, X. Cao, L. Bourgeois, *et al.*, *Adv Funct Mater*, 2012, **22**, 2682.
273. M. Zheng, D. Qiu, B. Zhao, *et al.*, *Rsc Adv*, 2013, **3**, 699.
274. G. Zhou, D.-W. Wang, L.-C. Yin, *et al.*, *Acs Nano*, 2012, **6**, 3214.
275. L. Renlong, C. Huaqiang, Q. Dong, *et al.*, *J Mater Chem*, 2011, **21**, 17654.
276. F. Zhang, H. Cao, D. Yue, *et al.*, *Inorg Chem*, 2012, **51**, 9544.
277. W. Wang, W. Lei, T. Yao, *et al.*, *Electrochim Acta*, 2013, **108**, 118.
278. Y. Su, S. Li, D. Wu, *et al.*, *Acs Nano*, 2012, **6**, 8349.
279. C. Zhang, X. Peng, Z. Guo, *et al.*, *Carbon*, 2012, **50**, 1897.
280. X. Zhang, P. S. Kumar, V. Aravindan, *et al.*, *J Phys Chem C*, 2012, **116**, 14780.
281. K. R. Paton, E. Varrla, C. Backes, *et al.*, *Nat Mater*, 2014, **13**, 624630.
282. Y. Gao, W. Shi, W. Wang, *et al.*, *Ind Eng Chem Res*, 2014, **53**, 2839.

RSC Advances Accepted Manuscript

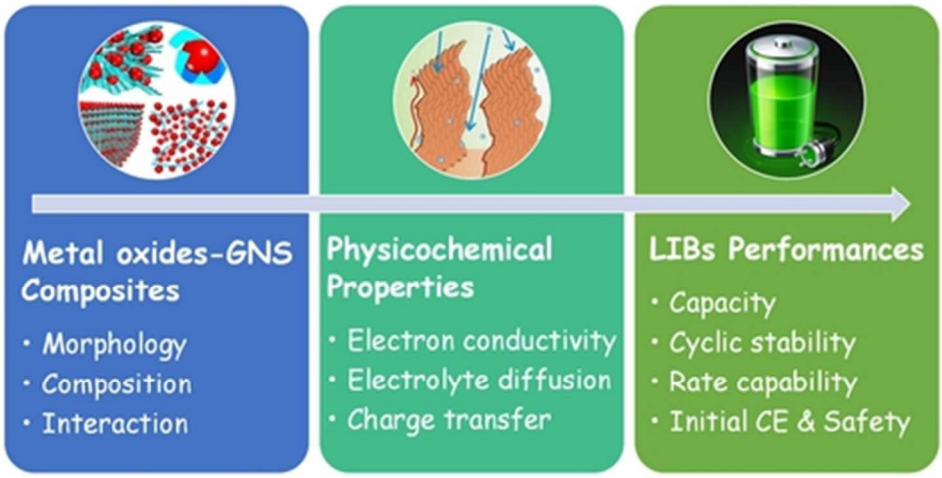

The review focuses on the effects of morphology, composition and interaction of 3D metal oxides-graphene composites on the performances of LIBs.
39x19mm (300 x 300 DPI)

RSC Advances Accepted Manuscript